

Characterization of a High Throughput Human Stem Cell Cardiomyocyte Assay to Predict Drug-Induced Changes in Clinical Electrocardiogram Parameters

Peter Kilfoil*¹, Lily Feng¹, Asser Bassyouni¹, Tiffany Lee¹, Derek Leishman³, Dingzhou Li², David J MacEwan⁴, Parveen Sharma⁴, Eric Watt² & Stephen Jenkinson¹.

Worldwide Research and Development, Pfizer Inc., La Jolla, CA 92121¹ and Groton, CT 06340², USA

Lilly Research Laboratories, Eli Lilly and Company, Indianapolis, IN 46285, USA³

Department of Pharmacology and Therapeutics, Institute of Systems, Molecular and Integrative Biology, University of Liverpool, L69 3GE, UK⁴

*Corresponding author: Peter Kilfoil, Pfizer Inc., 10646 Science Centre Drive, San Diego, CA 92121, USA

E-mail address: Peter.Kilfoil@pfizer.com

Tel +1 720 985 4372

Fax +1 858 678 8290

Running Title: High Throughput Human Stem Cell Cardiomyocyte Assay

Word Count:

Abstract	241
Introduction	550
Methods	3003
Results	2542
Discussion	1456

Abbreviations:

APD: Action potential duration

AUROC: Area under the receiver-operator curve

CiPA: Comprehensive *in vitro* proarrhythmia assay

ECG: Electrocardiogram

EFTPC: Effective free therapeutic plasma concentration

hERG: human ether-a-go-go-related gene

hiPSC-CM: human induced pluripotent stem cell cardiomyocyte

TdP: Torsades de Pointes

What is already known

- Stem cell cardiomyocytes can play a valuable role in the preclinical assessment of arrhythmia risk for development compounds
- Previous focus has been on the ability to predict of Torsades de Pointes (TdP) in an acute setting

What this study adds

- Generation of a high throughput clinically translatable hiPSC-CM model that can predict biologically relevant changes in QTc and QRS intervals of the ECG, as well define TdP risk.
- Model allows for extended incubation periods in serum free conditions, allowing assessment of long-term risks that may not be highlighted with acute treatment.

What is the clinical significance?

- The model allows for broader early assessment of cardiac risk of potential development compounds and will play a key role in reducing compound attrition in early clinical studies.

Abstract

Background and Purpose: Stem cell cardiomyocytes (hiPCS-CM's) play an increasingly important role in the safety profiling of candidate drugs. Specifically, such models are used for their ability to highlight the potential risk of arrhythmia generation that in most cases occur due to ion channel inhibition. For such models to have utility a clear understanding of clinical translation is required.

Experimental Approach: Using a high throughput serum free voltage sensitive dye platform we examined a diverse set of clinical compounds in our hiPCS-CM model, following acute (30 min) and chronic (24 h) incubations. Multiple assay parameters were examined to determine their ability to define clinical endpoints including QTc and QRS intervals of the ECG, and Torsades de Pointes (TdP) risk.

Key Results: Changes in hiPCS-CM threshold APD₉₀ values correlated with clinical compound plasma exposures producing QTc changes (Pearson $r^2 = 0.80$). In addition, a randomForest model using the stem cell data showed high predictivity in defining TdP risk (AUROC value = 0.938). Risk associated with QRS prolongation correlated with an increase in the rise time of the action potential (AUROC value = 0.982).

Conclusion and Implications: The in-depth understanding of the clinical translatability of our hiPCS-CM model positions this assay to play a key role in defining cardiac risk early in drug development. Moreover, the ability to perform longer term studies enables the detection of compounds that may not be highlighted by more acute assay formats, such as inhibitors of hERG trafficking.

Keywords: Action Potential; Clinical; QTc; Stem cell; Torsades de Pointes

1. Introduction

Development of in vitro assay systems that provide clinically translatable assessments of risk is a key goal within the pharmaceutical industry. One area that has received particular attention is the use of human induced pluripotent stem cell derived cardiomyocytes (hiPSC-CM) in defining cardiac safety (Gintant et al., 2020). hiPSC-CM express many of the same predominant depolarizing and repolarizing ion channels that shape the action potential in the human heart (Zhao et al., 2018), as well as well as other components whose functions modulate cellular membrane potential, and thus cardiac excitability. As such, hiPSC-CM represent a promising platform for investigating the integrated effects of drugs on the cardiac action potential. However, it should be noted that hiPSC-CM's show an immature phenotype (Ivashchenko et al., 2013; Zhu, Santana & Laflamme, 2009) and consist of mixed population of cardiac cell types (ventricular, atrial and nodal) (Ma et al., 2011). Hence although promising as an early in vitro model, the translatability of such a cell system with respect to clinical endpoints is still not fully defined.

Historically, in vitro safety profiling has heavily leveraged the testing of a compound's ability to block the human ether-a-go-go-related gene (hERG) potassium channel when addressing a compounds impact on cardiac electrophysiology (Food & Drug Administration, 2005). Blockade of the hERG channel is associated with a delay in cellular repolarization that is observed as a prolongation of the QT of the electrocardiogram (ECG), and the potential generation of cardiac arrhythmias. hERG inhibition alone, however, may overestimate the proarrhythmic liability of a compound and prevent low risk candidate molecules from progressing through development (Johannesen et al., 2014). Such disconnects may arise when a compound blocks additional cardiac currents, particularly the inward L-type calcium ($I_{Ca,L}$) and sodium (I_{Na}) currents, that may balance hERG-mediated reduction in the repolarizing current. Thus, drugs that show mixed ion channel

effects (MICE) may maintain the delicate balance of outward and inward currents driving repolarization.

In recent years the FDA-supported Comprehensive In Vitro Proarrhythmia Assay (CiPA) project has aimed to develop clinically translatable assays to predict arrhythmia generation (Colatsky et al., 2016; Fermini et al., 2016). One pillar of this approach has focused on hPSC-CM assays, and as such, groups have employed a wide array of methodologies to examine their potential in this respect, with efforts primarily focused on predicting Torsade de Pointes (TdP) risk (Ando et al., 2017; Blinova et al., 2018; Gintant, Fermini, Stockbridge & Strauss, 2017; Gintant et al., 2020; Gintant & Traebert, 2020; Kanda, Yamazaki, Osada, Yoshinaga & Sawada, 2018; Millard et al., 2018; Pfeiffer-Kaushik et al., 2019; Ribeiro et al., 2019).

In the present study we have validated a high throughput assay that allows for the simultaneous measurement of hPSC-CM action potentials in a 96 well format using a voltage-sensitive dye in combination with a fast-optical plate reader. The assay allows for the profiling of compounds in serum free conditions over an extended incubation period of up to 24 h, allowing for the detection of slowly manifesting effects, such as hERG trafficking block. Using this system, we have profiled a diverse set of clinical compounds to characterize the translation of several key clinical endpoints including QT and QRS intervals of the ECG, as well as TdP risk, thus highlighting the clear utility in early preclinical cardiac safety assessment of novel drug candidates.

2. Methods

2.1 Culture of hiPSC-CM's

Cryopreserved iCell² hiPSC-CM's (Cellular Dynamics International, Madison, WI, USA) were thawed and cultured in black walled optically clear plastic bottomed 96 well plates (Corning, Corning, NY, USA). Prior to seeding, wells were coated with 10 $\mu\text{g}\cdot\text{mL}^{-1}$ bovine fibronectin (Sigma-Aldrich, St. Louis, MO, USA) for one hour at 37°C. Following media removal, cells were plated (50,000 cells per well: 100 μL per well) in iCell² plating media (Cellular Dynamics International, Madison, WI, USA). Cells were cultured at 37 °C in a humidified environment (5% CO₂/95% air). After 24 h, 100 μL of iCell² maintenance media (Cellular Dynamics International, Madison, WI, USA) was added to each well. Following an additional 24 h incubation the media was exchanged for maintenance media (200 μL per well). The maintenance media was subsequently exchanged every 2 to 3 days. Cells were cultured for a total of 8 days by which time they had formed an electrically coupled monolayer with synchronous beating.

2.2 Gene expression analysis

Human Cardiomyocyte samples were obtained from Anabios Corporation (San Diego, CA, USA). All human hearts used for this study were non-transplantable and ethically obtained by legal consent (first person or next of-kin) from organ donors in the United States. All recovery protocols were preapproved by the Institutional Review Boards (IRB) at each transplant center and the procurement processes are fully traceable and periodically reviewed by US Federal authorities. Upon arrival in the laboratory, hearts were re-perfused with an ice cold proprietary cardioplegic solution as previously described (Page et al., 2016). Adult human primary ventricular myocytes were isolated enzymatically from the ventricles. Digestion of the cardiac tissue was conducted at 37°C for 25 min utilizing a proprietary solution which included a cocktail of proteolytic enzymes

(Nguyen et al. 2017). Isolated cells were provided for this study as pellets snap-frozen in liquid nitrogen after isolation.

Total RNA was isolated from human primary ventricular myocytes and harvested iCell² hPSCs using a Qiagen RNeasy micro kit (Qiagen, Germantown, MD, USA) in accordance with the manufacturer's protocol. Extracted RNA was quantified using a NanoDrop ND-1000 spectrophotometer (Thermo Fisher Scientific, Wilmington, DE, USA). The quality and quantity of the extracted RNA was assessed using an Agilent 4200 TapeStation system (Agilent Technologies, Santa Clara, CA, USA). First strand, then second strand cDNA was synthesized, amplified, fragmented, labeled, and hybridized using the Clariom D assay kit according to the manufacturer's protocol (Affymetrix, Santa Clara, CA, USA). The samples were prepared for hybridization and transferred to the GeneChip cartridge arrays. Arrays were incubated for 16 h in an Affymetrix GeneChip 645 hybridization oven at 45°C with rotation at 60 rpm. The arrays were washed and stained using the Affymetrix GeneChip Fluidics Station 450. Finally, the arrays were scanned using an Affymetrix GeneChip Scanner 3000. Data was primarily analyzed using the Affymetrix Transcriptome Analysis Console software.

2.3 Measurement of cellular action potentials in hPSC cardiomyocytes

High throughput measurements of hPSC-CM's action potentials were acquired optically using a fluorescent voltage sensitive dye methodology and the Photoswitch Bolt fast kinetic plate reader (Photoswitch Biosciences, Cleveland, OH, USA). This technology allows for simultaneous measurement of fluorescence changes across a 96 well assay plate at a capture rate of 10 kHz, thus allowing for a high-resolution capture of changes in the membrane potential.

The voltage sensitive dye used in this study, PhoS-VSD (Photoswitch Biosciences, Cleveland, OH, USA), was dissolved at a concentration of 500 nM in serum-free FluoroBrite DMEM (Thermo

Fisher, Waltham, MA, USA) containing HEPES (20 mM). Following media aspiration, the dye solution was added to each well (100 μ L per well) and the plate was incubated for 15 min at 37°C. The dye solution was subsequently removed and replaced with 180 μ L of recording media (FluoroBrite DMEM/ HEPES (20 mM)). The plate was returned to the cell culture incubator for 30 min before being placed in the Photoswitch Bolt instrument for an additional 30 min to allow for temperature equilibration. The instrument temperature was set at 28°C. Measurement of the temperature across randomly selected wells (N=10) demonstrated a mean assay plate temperature of 28°C with a standard deviation of 0.1°C after this 30 min incubation period.

Test compounds were dissolved and initially diluted in dimethyl sulfoxide (DMSO). Subsequent dilutions were then prepared in recording buffer, providing for 10x test solutions. Upon compound addition (20 μ L) the final DMSO concentration in the assay was 0.1% (v/v). Each compound was tested across a range of 10 concentrations.

During the assay, cells were excited at 660 nm and the change in fluorescence over time was measured. A 40 s baseline reading was obtained prior to the addition of test compounds. After addition of test compounds, the cells were equilibrated in the instrument for a further 30 min before a second 40 s read was performed. Assay plates were then returned to the incubator before being removed and returned to the Photoswitch Bolt 30 min prior to the final 24 h read. Fluorescent signals were analyzed using the proprietary analysis software from Photoswitch (version 1.1.7.27239), enabling the measurement of action potential duration (APD), beat rate and rise time for each well.

2.4 hERG fluorescent polarization binding assay

Human embryonic kidney (HEK) cells stably transfected with a doxycycline inducible plasmid expressing the hERG channel (Accession Number: NM_000238) were cultured in suspension in Ex-cell 293 Serum Free Medium containing fetal bovine serum (5% v/v), L-Glutamine (6 mM), Blasticidin ($5 \mu\text{g}\cdot\text{mL}^{-1}$) and Zeocin ($600 \mu\text{g}\cdot\text{mL}^{-1}$) at 37°C in a humidified environment (5% $\text{CO}_2/95\%$ air). hERG expression was induced by the addition of doxycycline ($1 \mu\text{g}\cdot\text{mL}^{-1}$) 48 h prior to harvesting by centrifugation. Cell pellets were resuspended in ice cold homogenization buffer (1 mM EDTA, 1 mM EGTA, 1 mM NaHCO_3 , and cOmplete™ protease Inhibitor cocktail). Cells were homogenized using a dounce homogenizer (20 strokes), and centrifuged ($1,000\times g$) for 10 min at 4°C . The supernatant was transferred to a new tube and was centrifuged a second time ($25,000\times g$) for 20 minutes at 4°C . The supernatant was discarded, and the pellet was resuspended in buffer (50 mM HEPES, 10 mM MgCl_2 , bovine serum albumin (0.2% w/v) and cOmplete™ protease inhibitor cocktail). The samples were adjusted to $5 \text{ mg}\cdot\text{mL}^{-1}$ and frozen.

For the assay, membrane aliquots were thawed on ice and diluted to $200 \mu\text{g}\cdot\text{mL}^{-1}$ in assay buffer (25 mM HEPES, 15 mM KCl, 1 mM MgCl_2 , and 0.05% (v/v) Pluronic F127). A Cy3B tagged N-desmethyl dofetilide ligand was prepared in the same assay buffer solution (5 nM). Compound or vehicle (DMSO) was spotted into each well of a black 384-well low-volume plate. Membrane homogenate (15 μL) and Cy3B tagged ligand (10 μL) were then added to each well and the plate was incubated at room temperature for 16 h. Fluorescence polarization measurements were made using an Envision plate reader (Perkin Elmer) and mP values were used for analysis. Binding K_i values were determined using the Cheng-Prusoff equation ($K_i = \text{IC}_{50}/(1+L/K_d)$), where L was the labelled ligand concentration in the assay (2 nM), and the K_d value (1.35 nM) the affinity constant for the labelled ligand (Cheng & Prusoff, 1973).

2.5 Ion channel profiling

Chinese hamster ovary (CHO) cells stably expressing human Cav1.2/ β 2/ α 2 δ 1 calcium channel (Catalogue No. CT6004; Charles River Cleveland, OH, USA) were cultured in Ham's F12 medium supplemented with fetal bovine serum (FBS; 10% (v/v)), G418 (0.25 mg.mL⁻¹), hygromycin (0.25 mg.mL⁻¹), zeocin (0.4 mg.mL⁻¹), and blasticidin (0.01 mg.mL⁻¹). On the day prior to cell harvest, tetracycline (1 μ g.mL⁻¹) was added to the media to induce channel expression and the calcium channel antagonist verapamil (15 μ g.mL⁻¹) was added to minimize calcium-induced cytotoxicity. CHO cells stably expressing the human Nav1.5 sodium channel (Catalogue No. CT6007; Charles River Cleveland, OH, USA) were cultured in Ham's F12 media supplemented with 10% FBS (10% (v/v) and G418 (0.25 mg.mL⁻¹).

All cell lines were cultured at 37 °C in a humidified environment (5% CO₂/95% air). On the day of the experiment, cells were harvested at 70-80% confluency by rinsing with Hank's Balanced Salt Solution and incubating for 2 min in Accutase (Innovative Cell Technologies, San Diego, CA, USA). Cells were resuspended (2 million cells per mL) in CHO-S-SFM II serum-free medium supplemented with 20 mM HEPES and were allowed to recover for 45 min with constant stirring prior to electrophysiological measurements. All tissue culture media and reagents were obtained from Thermo Fisher (Waltham, MA, USA), unless otherwise stated.

Ionic currents were evaluated in the whole-cell configuration using the Qube384 automated planar patch clamp platform (Sophion Bioscience A/S, Ballerup, Denmark). QChip 384X plates, containing 10 patch clamp holes per well, were used to maximize success rate, which was routinely > 95%.

For Cav1.2 experiments, the external solution was composed of (in mM): 137.9 NaCl, 5.3 KCl, 0.49 MgCl₂, 10 CaCl₂, 10 HEPES, 0.34 Na₂HPO₄, 4.16 NaHCO₃, 0.41 MgSO₄, 5.5 glucose, pH 7.4, 312 mOsm.kg⁻¹. The internal solution contained (in mM): 27 CsF, 112 CsCl, 2 MgCl₂, 10 EGTA, 10 HEPES, 2 Na₂ATP, pH 7.2, 307 mOsm/kg. For Nav1.5 experiments, the external solution was composed of (in mM): 137.9 NaCl, 5.3 KCl, 0.49 MgCl₂, 1.8 CaCl₂, 10 HEPES, 0.34 Na₂HPO₄, 4.16 NaHCO₃, 0.41 MgSO₄, 5.5 glucose, pH 7.4, and osmolarity of 303 mOsm.kg⁻¹. The internal solution contained (in mM): 92 CsF, 55 CsCl, 2 MgCl₂, 5 EGTA, 5 HEPES, 1 MgATP, pH 7.2, 298 mOsm.kg⁻¹. The osmolarity of the buffer was adjusted by the addition of sucrose as required.

The Cav1.2 current was elicited by a voltage step to 0 mV for 150 ms from a holding potential of -40 mV. Voltage steps were repeated at 0.05 Hz, and Cav1.2 amplitude was measured as the peak current at 0 mV. For the Nav1.5 current, from an initial holding potential of -80 mV, a 200 ms prepulse to -120 mV was used to homogenize channel inactivation, followed by a 40 ms step to a test potential of -15 mV. Membrane potential was further depolarized to +40 mV for 200 ms to completely inactivate the peak Nav1.5 current, followed by a ramp from +40 mV to -80 mV (-1.2 mV.ms⁻¹). This voltage pattern was repeated at 0.2 Hz, with the Nav1.5 peak current defined as the maximum current during the step to -15 mV. All studies were conducted at 23°C.

Compounds were initially dissolved and diluted in DMSO, with a final dilution by the addition of external solution to generate final working concentrations. The final DMSO concentration in all experiments was 0.33% (v/v). Three vehicle periods each lasting 5 minutes were applied to establish a stable baseline, each well subsequently received a single concentration of compound. This application was repeated three times for each well, via a flowthrough addition where the solution was replaced with each addition. Each exposure lasted 10 minutes.

Patch clamp data were analyzed using Assay Software (Version 6.4.72; Sophion Bioscience A/S, Ballerup, Denmark). Current amplitudes were determined by averaging the last 4 currents under each test condition. The percent inhibition of each compound was determined by taking the ratio of current amplitude measured in the presence of various concentrations of the test compound (I_{Compound}) versus the vehicle control current (I_{Vehicle}):

$$\% \text{ Inhibition} = [1 - (I_{\text{Compound}}/I_{\text{Vehicle}})] * 100\%.$$

A dose-response curve was generated IC_{50} value defined for each compound by fitting the data to a four-parameter logistical equation using the Sophion Analyzer software. The minimum response and slope were free fitted and maximum response was fixed to 100%.

2.6 Materials

All compounds were obtained from Sigma-Aldrich (St. Louis, MO, USA) with the exceptions of Mesoridazine, (ApexBio, Houston, TX, USA), Ribociclib (Tocris Bioscience, Minneapolis, MN, USA) and Vandetanib (Cayman Chemical Company, Ann Arbor, MI, USA).

2.7 Clinical Data

Clinical concentration-QTc relationships were gathered from reference sources (Supplemental Table 2). Many of the studies highlighted had explicit concentration-QTc slopes or pharmacokinetic/pharmacodynamic (PK/PD) models described. These formulae were used to calculate QTc changes for a range of free plasma exposure concentrations that had been explored in the original reports (interpolation, rather than extrapolation). In some cases, concentration-QTc data were presented in a figure format within the paper or report, with or without a linear regression line for concentration-QTc. If a line was available this was digitized to extract slope data. When only concentration-QTc pairs were plotted these data were also digitized and a linear

regression was used to calculate the slope of the concentration-QTc relationship. This slope was used to calculate QTc values for a similar concentration range to that explored in the published study. Finally, some data were only available in the publications as limited discrete concentration and QTc datapoints where no slope could be practically estimated. These data were used as is. The concentrations were changed to molar units using molecular weight information from DrugBank (DrugBank.com) and the unbound concentration was calculated using publicly available plasma protein binding data (DrugBank, US product labels, FDA approval documents, or rarely separate publications). For a summary of the calculated free plasma exposures producing a 10 ms change in QTc, and the associated references, see Supplemental Table 2

For a full description of the effective free therapeutic plasma concentration (EFTPC) for each compound, defined as the concentration of unbound compound in the plasma at a therapeutic dose, and associated references see Supplemental Table 3.

2.8 Curve Fitting and Modeling

For hiPSC-CM studies, responses generated in compound treated wells were normalized to two vehicle controls wells located on the same row of the plate. Multiple endpoints including APDs, beat rate, and rise time, were assessed for each well. This measurement was repeated at 30 minutes and 24 hours.

The readout of a measurement was normalized to vehicle control wells of the curve via:

$$\text{Response} = \text{Readout}/\text{Mean (Vehicle)} - 1$$

For each readout the data were further normalized by subtracting the median response value of the lowest two concentrations of all compounds. Response values from treatment groups

annotated as having arrhythmia class 4-5 (see Supplemental Data 2 for details on arrhythmia classification) were removed prior to curve fitting. Models were fit using methods described in (Filer, Kothiya, Setzer, Judson & Martin, 2017) with modifications. The hill and gain-loss objective functions, optimized using maximum likelihood and a student's t distributed error model, were fit in R 3.6.2 (R-Project, 2019) using the nloptr package to access NLOpt 2.4.2 (Johnson, 2017) with optimization performed using the BOBYQA algorithm (Powell, 2009). The best model was selected based on the lowest AIC (Akaike, 1998).

Determining the free plasma drug exposure required to produce a 10 ms change in the clinical QTc was performed using the same methodology as above, with the exception that the data were not normalized.

Torsades de Pointes (TdP) risk categories were defined primarily using the definitions provided by CredibleMeds.org and by CiPAPProject.org. For a full description of the TdP risk categorization used in this study, and associated references, see Supplemental Table 4. Drugs categorized as a 'Known Risk' (defined at category 1 in Supplemental Table 4) were considered TdP positive while all others were considered TdP negative.

All machine learning models were generated using Caret 6.0-86 (Kuhn, 2020) and R 3.6.2 (R-Project, 2019). To determine the predictive performance of the models, 20 times repeated 5-fold cross validation was performed on each model. Features used in the models included curve fit parameters (hill top, margin to the threshold concentration) and curve response values at multiples of the EFTPC for all of the hIPSC-CM endpoints. Ion channel inhibition data (binding for hERG and patch clamp for Cav1.2 and Nav1.5) was also incorporated into the modeling. This included direct ion channel inhibition percentages, as well as metrics calculated from waveforms

generated by an in silico cardiomyocyte model (O'Hara, Virag, Varro & Rudy, 2011) using an epicardial cell type at 60 beats per minute, and the exposure margin necessary to observe a 10 ms increase in the cardiomyocyte model APD₉₀. Features were explored individually and in combination using a variety of machine learning algorithms. These include logistic regression (stats package in base R), elastic net from glmnet 4.1 (Friedman, Hastie & Tibshirani, 2010), randomForest 4.6-14 (Liaw & Wiener, 2002), and recursive partitioning and regression trees from rpart 4.1-15 (Therneau & Atkinson, 2019).

2.9 Data and Statistical Analysis

This manuscript has followed the recommendations set out in the *BJP* editorials wherever relevant. The data and statistical analysis comply with the recommendations of the *BJP* on experimental design and analysis in pharmacology (Curtis et al., 2018). Statistical analysis was undertaken only using independent values where $n \geq 5$.

Gene expression data were analyzed by means of an F-test to determine significant differences in gene expression across the whole data set using Transcriptome Analysis Console Software v4.0.1.36 (Thermo Fisher Scientific, Waltham, MA, USA). For comparisons of the expression of a specific target gene between iCell² and human ventricular cells a Welch's *t*-test was performed (Welch, 1947). Pearson correlation analysis of all non-censored data was performed using GraphPad Prism v9.00 software (RRID:SCR_002798, <http://www.graphpad.com>). A correlation comparison of non-censored or non-censored/censored data was performed using a Spearman rank analysis (Spearman, 1987). In all cases a *P* value of <.05 was considered significant. *n* indicated the number of individual experiments or tissue samples.

To understand the ability of the hiPSC-CM model APD₉₀ threshold values in predicting the clinical exposures producing a 10 ms QTc change or the IC₅₀ concentration in the calcium patch clamp assay linear regression modeling was performed using a 4-fold cross validation with 10 repetitions. Performance metrics including the r² value and the root mean square error (RMSE) were reported. Similarly, a 5-fold cross validation was performed using hiPSC-CM rise time values and the ratio of the clinical exposure associated with QRS prolongation/EFTPC to determine the predictivity of the assay with respect to defining clinical QRS risk.

Receiver-operator curve analyses that were not associated with the modeling efforts were performed using a webtool previously described by Goksuluk et al. (Goksuluk, Krokamaz, Zararsiz & Karaagaoglu, 2016).

2.10 Nomenclature of target and ligands

Key protein targets and ligands in this article are hyperlinked to corresponding entries in <http://www.guidetopharmacology.org>, the common portal for data from the IUPHAR/BPS Guide to PHARMACOLOGY (Harding et al., 2018), and are permanently archived in the Concise Guide to PHARMACOLOGY 2019/20 (Alexander et al., 2019).

3. Results

3.1 GeneChip expression analysis

Gene expression was compared between iCell² hiPSC-CM's and purified human primary ventricular cardiomyocytes obtained from donor tissue (Supplementary Table 1). From a total of 48,243 transcripts, 37,494 (77.7%) did not significantly differ in expression between the two cell types, 6,785 transcripts (14.1%) were significantly upregulated, and 3,964 transcripts (8.2%) were

significant downregulated in iCell² cells compared with human primary cardiomyocytes (Figure 1a).

Several ion channels involved in the generation of the cardiomyocyte action potential, including KCNH2 (hERG) and CACNA1C (Cav1.2 calcium channel), showed similar expression levels (figure 1b). Differences in expression were observed for KCNJ2 (responsible for I_{K1} current) and KCND3, (responsible for I_{to} current), where expression of both was lower in the iCell² cardiomyocytes (12.4 and 8.7-fold, respectively). SCN5A (Nav1.5 sodium channel) expression was significantly higher in the iCell² cardiomyocytes; however, the absolute difference was small in magnitude (1.5-fold increase).

3.2 Measurement of hIPSC-CM action potential parameters

hIPSC-CM action potentials (APs) were examined in voltage-sensitive dye-loaded cells. At an acquisition rate of 10kHz, signals were captured at a resolution equivalent to those obtained by traditional patch clamp techniques, making it possible to accurately measure a wide variety of endpoints (Figure 2a, b and c). Treatment with the hERG channel blocker dofetilide produced a prolongation in the repolarization (Figures 2a, 2d and 2g) following a 30 min or 24 h incubation. At 24 h higher concentrations of dofetilide (>10 nM) led to significant tachyarrhythmias (Figure 2g). The calcium channel blocker nifedipine shortened the action potential duration (APD) at both time points (figures 2b, 2e and 2h) and the hERG trafficking blocker pentamidine had no effect on APD acutely, but did delay the repolarization after a 24 h incubation, in line with the membrane turnover of the hERG channel ($T_{1/2}$ of ~11 hours) (Ficker, Dennis, Wang & Brown, 2003).

QT interval of the ECG and APD are rate dependent. Compound effects on QT interval can be corrected to beat rate using one of several correction formulae, such as Bazett's (Bazett, 1920) or

Fridericia (Fridericia, 1920). An additional correction recently proposed by Yamamoto et al. (Yamamoto et al., 2016), has been suggested to be more suited for use with hIPSC-CM's. Figure 2j highlights the distribution of APD₉₀ measurements from vehicle treated cells compared to their corresponding RR interval (beat to beat interval). APD₉₀ refers to the time required for the action potential to repolarize by 90%. As expected, as the beat rate slows, and the RR interval increases, the APD₉₀ values increase. Employing Bazett's, Fridericia's or Yamamoto's formulae resulted in a correction in APD₉₀ (Figures 2k and 2l). The vehicle treated correlation generated a slope of 0.130 ± 0.005 , which was reduced to -0.010 ± 0.003 using Bazett's, 0.022 ± 0.004 with Fridericia's and -0.005 ± 0.003 with Yamamoto's correction formulae. With the resultant slope being the closest to zero, the Yamamoto correction was deemed the most appropriate correction formula for the present study.

3.3 Correlation of hIPSC-CM action potential duration to clinical QTc interval

A key aim in the development of an in vitro hIPSC-CM model is the ability to predict compound-mediated clinical QTc interval changes. With the expression of multiple ion channels involved in the generation of the cardiac AP present in this cell based system, it has the potential to be able to predict not only QTc changes associated with selective hERG channel blockers, but also integrated responses for compounds that possess multi-ion channel pharmacology. With that goal, 29 compounds were selected for which clinical QTc data were available (Table 2). Concentration-response curves were generated for each compound in the hIPSC-CM model and the concentration of each compound that produced a positive threshold increase in APD₉₀ was determined (defined as three times the standard deviation of the vehicle control, which equated to an increase of 10.3 % and 7.94 % from baseline for the 30 min and 24 h time points, respectively). All curve fitting was performed using an automated curve fitting algorithm to avoid bias. A single curve fit was

performed per compound using a combined APD₉₀ data set ($n \geq 3$ independent experiments per compound). A similar method was used to define the compound exposure required to produce a 10 ms increase in the clinical QTc interval (Table 1).

Pearson correlation analyses were performed comparing various endpoints that included APD₉₀, Yamamoto-corrected APD₉₀ (cAPD₉₀), clinical QTc data and hERG binding data (Figure 3). Since not all compounds reached the defined threshold value (i.e. data where values have a > prefix, defined here as censored values), we also performed Spearman rank correlation analyses to ensure that both non-censored and censored data were included in the analysis (Table 2). An excellent correlation was observed between the concentration of compound producing a threshold increase in hIPSC-CM APD₉₀ and the concentration producing a 10 ms increase in the clinical QTc interval (Figure 3a). Statistical analysis using either a Pearson or Spearman rank correlation highlighted that the 24 h timepoint in the hIPSC-CM assay correlated more closely with the clinical QTc than the corresponding 30 min timepoint (Table 2). Correlations were similar when comparing cAPD₉₀ values (Figure 3b), or when hERG binding pK_i values were substituted for the APD₉₀ values (Figure 3c). In addition, there was also a robust correlation between APD₉₀ and hERG pK_i values (Figure 3d) whether looking more specifically at the smaller subset of compounds that had associated clinical QTc data available (24 h timepoint: $r^2 = 0.757$; $n = 23$) or the larger compound set used in this study ($r^2 = 0.718$; $n = 42$).

In addition, to determine the ability of the hIPSC-CM model or the hERG binding to predict a 10 ms change in the clinical QTc interval a 4-fold cross validation analysis was performed using APD₉₀ threshold (increase) values or hERG pK_i values. For the hIPSC-CM APD₉₀ values the r^2 value was 0.84 (i.e. the data explain 84% of the variability in the clinical QTc data) with a root mean square error (RMSE) of $\text{Log}_{10} = 0.64$, which translates to an error of 4.4-fold. In contrast

for hERG pK_i values the r² value was slightly higher at 0.86 with a RMSE of Log₁₀ = 0.60 , which translates to an error of 4.0-fold. Using the Pearson correlation of non-censored data allowed for the generation of correlation equations for each assay (Table 2), that can be used to define an estimation of the clinical QTc effects using either hIPSC-CM or hERG pK_i endpoints.

3.4 Prediction of TdP risk using hIPSC-CM endpoints

Several features from the hIPSC-CM assay endpoints were evaluated for their ability to predict clinical TdP. These include curve fit parameters (Hill top) and values calculated from the Hill model in the context of the EFTPC. The latter includes the margin between the plasma concentration and the concentration at which the Hill model crosses the baseline threshold for that endpoint. In addition, response values at 1, 3, 10, 30, and 100 times the EFTPC were calculated from the hill model. These are labeled as MRYYx with the ‘YY’ indicating the multiple (i.e. MR30x for maximal response at 30x EFTPC).

Models constructed using individual response values at multiples of EFTPC were predictive, with area under receiver-operator curve (AUROC) values in the range of 0.84 to 0.92 for the most predictive models trained using categorization trees and logistic regression. These models consistently found higher AUROC values from APD_{50/80/90} endpoints, with a slight benefit to the corrected APD values. The MR30x values were among the most predictive.

Combinations of features were explored to see if model performance could be improved. An elastic net model trained on all maximal response values had a AUROC of 0.885; limiting to just the MR30x values had a similar performance (AUROC of 0.899). Further improvement was found using randomForest models on subsets of the more predictive features. Ultimately the optimal model, with both the highest AUROC (0.938) and Matthew’s Correlation Coefficient (MCC)

(0.736) (Matthews, 1975), was a randomForest model trained using the MR30x values from the cAPD₉₀ and cAPD₅₀ endpoints from the 24 h time point, as well as the Hill top values from the same curves (Table 3 and Figure 3e).

Results from the ion channel assays were also explored. Ion channel blocks were calculate as described in (Lancaster & Sobie, 2016) and were used in the O'Hara-Rudy cardiomyocyte model to generate membrane potential and calcium waveforms (O'Hara, Virag, Varro & Rudy, 2011). These were run at a wide range of assumed drug concentrations to generate waveforms at multiples of the EFTPC, and the compound concentrations producing a 10 ms change in APD₉₀ were calculated. Subsequent modeling analysis included ion channel block values directly, metrics calculated from the waveforms as described in (Lancaster & Sobie, 2016), and the margin necessary to generate a 10 ms APD₉₀ increase.

Ion channel features alone were not as predictive as models trained on the stem cell data. Incorporating ion channel features with the stem cell data did not generate models that were more predictive than the stem cell features alone (Table 3).

To contextualize the results of the optimal model, we explored partial dependency plots (Greenwell, 2017) (Figure 3f). A detailed summary of the prediction of each compound in each model can be found in Supplemental Figure 1.

3.4 Translation of hIPSC-CM's action potential rise time to clinical QRS prolongation

Cardiac sodium channels, such as Nav1.5, are essential for the rapid depolarization that initiates a ventricular AP, and their inhibition results in a prolongation of the QRS interval of the ECG. If pronounced enough this has the potential lead to cardiac arrhythmias (Tan, Bezzina, Smits, Verkerk & Wilde, 2003). Here we examined AP rise time (i.e. time from the initiation of

depolarization to the maximum depolarization), as a surrogate of sodium channel inhibition, to determine if this endpoint was predictive of clinical QRS prolongation. We compared the compound concentration required to produce a threshold increase in AP rise time (defined as three times the standard deviation of the control data, which equates to a change of 1.72% from baseline) with compounds that had been associated, or not associated, with QRS prolongation at a measured free plasma concentration. For several compounds profiled in this study an increase in AP rise time was not detected, however an abrupt cessation of beating was observed as the compound concentration was increased. Since the Hill slope of the inhibition of sodium channel activity can be steep, it is likely that this rapid transition from beating to quiescence is sodium channel mediated. In such cases the concentration selected for analysis was the geometric mean concentration that fell between where the cells showed normal AP morphology and those that were quiescent.

For compounds to be included in this analysis the clinical exposure data had to be time-matched with the observed QRS measurement. As with previous studies in this area (Harmer, Valentin & Pollard, 2011), due to the lack of extensive clinical studies focusing on QRS interval measurement, we expanded our criteria to include single case reports and reports of compound overdose, however the requirement for time-matched exposure/QRS measurements was maintained.

A total of 35 compounds were selected, 21 associated with QRS prolongation and 14 not associated (Table 4). For QRS positive compounds, the ratio of the concentration required to produce a threshold increase in AP rise time in the hIPSC-CM's over the lowest reported clinical exposure associated with QRS was calculated. For QRS negative compounds the ratio of the concentration producing an increase in threshold AP rise time over the highest reported exposure was defined. For many compounds this equated to their EFTPC that would be observed during normal

therapeutic use. These ratios were used in combination with a binary definition of QRS prolongation liability to perform a receiver-operator curve (ROC) analysis to determine if increases in hIPSC-CM AP rise time were associated prolongation of the clinical QRS interval. In addition, for comparison a similar analysis was performed using Nav1.5 patch clamp data, with the analysis being subdivided by the compound addition period. These equated to period 1 (one compound addition; 10 min total incubation), period 2 (two compound additions; 20 min total incubation) or period 3 (three compound additions; 30 min total incubation).

ROC analysis of the patch clamp data highlighted AUROC values of 0.974, 0.960 and 0.953 with respect to the data from the period 1, 2 and 3, respectively (Figure 4 and Table 5). Moreover, analysis of period 1 patch clamp data showed the highest-level sensitivity/specificity with values of 1.00 and 0.86, respectively, when using an optimal cut-off value defined using the ROC01 analysis methodology (Goksuluk, Krokamaz, Zararsiz & Karaagaoglu, 2016). hIPSC-CM AUROC values were slightly higher with an identical AUROC value of 0.982 observe for both the 30 min and 24 h time points (Table 5).

To determine the ability of the hIPSC-CM model to predict clinical QRS risk, a 5-fold cross validation analysis, repeated 10 times, was performed comparing AP rise time threshold values with the ratio of the clinical exposure associated with QRS prolongation/EFTPC in an ROC analysis. This analysis resulted in a decrease in the AUROC values for the patch clamp assay (0.918, 0.909 and 0.903 for the period 1, 2 and 3, respectively), however the hIPSC-CM data AUROC values were maintained with value of 0.980 (sensitivity/specificity: 0.941/0.837) at the 30 min time point.

3.5 Translation of hIPSC-CM's action potential duration to calcium channel inhibition

Calcium channel inhibition leads to a reduction in APD in cardiomyocytes (Lee, Hyun, Park, Kim & Kim, 2016). In the present study we examined the correlation between the concentration of compound required to produce a threshold reduction (defined as three times the standard deviation of the control data, which equates to an approximate change of 11% from baseline) in APD₉₀ versus IC₅₀ values for calcium current inhibition in a Cav1.2 patch clamp assay. All compounds from the broader compound test set that generated a threshold reduction in APD₉₀ were included in the analysis. A correlation was observed between uncorrected APD₉₀ threshold concentration values and calcium channel patch clamp IC₅₀ values ($r^2 = 0.80$; $n = 16$) (Figure 5a). In hPSC-CM's calcium channel antagonists are known to produce an increase in beat rate, an effect that is the opposite from what is observed in primary ventricular cardiomyocytes (Zeng, Wang, Clouse, Lagrutta & Sannajust, 2019). This effect was also observed in the present study where we found a correlation between the concentration of compound required to produce an threshold increase in beat rate values (defined as three times the standard deviation of the vehicle control data) with the calcium channel patch clamp IC₅₀ values ($r^2 = 0.67$; $n = 14$) (Figure 5b). Correcting the APD₉₀ values for the change in beat rate using the Yamamoto formula led to an improved correlation ($r^2 = 0.87$; $n = 17$) (Figure 5c).

To determine the ability of the hPSC-CM model to predict the calcium channel inhibition in the patch clamp assay, a 4-fold cross validation analysis was performed using cAPD₉₀ threshold (reduction) values. The r^2 value was 0.90 with an RMSE of $\text{Log}_{10} = 0.59$, which translates to an error of 3.9-fold. Hence, for compounds with predominant calcium channel antagonism pharmacology there is a clear predictive relationship with corrected APD₉₀ threshold values that follows the linear equation of $y = 1.021x + 0.932$.

4. Discussion

In recent years the pharmaceutical industry has explored the utility of hPSC-CM's in addressing potential cardiac risk(s) in early preclinical development. Such efforts focus on two main areas, arrhythmogenesis and changes in cardiac contractility. Cardiac arrhythmias arise due to changes in cardiac conduction and can be induced by ion channel block. Indeed, it is well known that inhibition of the hERG potassium channel results in a reduced rate of repolarization of the cardiomyocyte resulting in a prolongation of APD that in turn can lead to a potentially life threatening TdP arrhythmia.

Although hERG profiling is now routine in the development of novel drug candidates, there has been an increased focus on efforts to more fully define methodologies to assess arrhythmia risk that go beyond hERG to include other channels that play a role in the morphology of the cardiac AP. Such effort have been the focus of the FDA-supported CiPA project (CiPAproject.org; (Colatsky et al., 2016; Fermini et al., 2016)). One key component of CiPA is the use of hPSC-CM's based on the rationale that they represent an integrated system with a composite readout with respects to a compounds overall activity at multiple targets. Indeed, the value of hPSC-CM's has been recognized in recent discussion around the updating of ICH S7B regulatory guidelines (Anon, 2020).

For an hPSC-CM model to be valuable in early risk assessment there are several criteria the model should address. The model endpoints must show a robust translation to defined clinical endpoints. Ideally, the assay should be simple, robust and be amenable to high throughput screening to allow for profiling of larger compound sets. Moreover, serum free conditions are key to avoiding potential issues with compound protein binding. Finally, slow target on-rates, or compounds that

affect target expression over time, necessitate the need for an assay amenable to longer term incubations. Each of these points have been addressed in validation of our hPSC-CM model.

An additional consideration is the expression profile of targets involved in generating the cardiac AP. Although human derived, one cannot assume that hPSC-CM cells have the same expression profile as that observed in primary human adult ventricular cardiomyocyte. Indeed, hPSC-CM have been described to exhibit an immature electrophysiological phenotype, notably in their automaticity, lower upstroke velocity (secondary to depolarized diastolic potential) and less prominent phase 1 notch (Garg, Garg, Shrestha, Sanguinetti, Kamp & Wu, 2018). Hence, we compared the gene expression of the iCell² cardiomyocyte to purified human ventricular myocytes to investigate expressional differences responsible for these observed phenotypes. The expression of key genes such as those encoding hERG, Cav1.2 and Nav1.5 were similar between both cell types, providing confidence that compounds targeting such channels would produce a similar pharmacological response across both cell types. Interestingly, the expression of KCNJ2, the channel responsible to the I_{k1} current that plays an important role in maintaining the hyperpolarized resting potential of the adult ventricular myocardium, was lower in the iCell² cell type. This likely explains why this cell line has a more positive potential compared with primary ventricular myocytes (Perez-Hernandez et al., 2018). Similarly, KCND2, encoding the I_{to} current, was lower in iCell² cardiomyocytes, explaining the lack of a prominent phase 1 notch in these action potentials. As a whole, the expressional profile of these channels in iCell² is in agreement with previous studies which compared functional expression between hPSC-CM and adult cardiomyocytes (Garg, Garg, Shrestha, Sanguinetti, Kamp & Wu, 2018).

The aim of the current study was to assess the ability of our model to predict a variety of clinical endpoints, specifically QTc and QRS intervals of the ECG, as well the life threatening arrhythmia Torsade de Pointes (TdP).

Given the relationship between the QT interval and APD, the concentrations of a series of compounds required to produce a threshold positive change in APD₉₀ were correlated with the free clinical exposure producing a 10 ms change in the QTc interval. A robust correlation was observed that was not enhanced by using rate-corrected values. The linear nature of the correlation allows for the prediction of the clinical exposures producing a 10 ms change in QTc from hIPSC-CM data. Interestingly, given the diverse compound set used in this study, the hERG binding assay was slightly better at predicting QTc. Moreover, a comparison of the larger compound set, where not all compounds had published clinical QTc data, showed a robust correlation of the APD₉₀ positive threshold concentration with the hERG binding K_i value, similar to previously reported findings for hERG patch (Saxena et al., 2017).

The ability of a compound to inhibit the hERG channel is closely linked to QTc prolongation and this in turn is related to an increased risk of TdP (Roden, 2004). However, hERG inhibition alone is not the sole determinant of TdP liability. For example, verapamil, used clinically as a calcium channel antagonist to treat high blood pressure, also blocks hERG at a similar IC₅₀. The calcium channel block offsets the hERG-induced APD prolongation and as such this compound is not associated with an increase in QTc interval or TdP risk in the clinical. Therefore, for compounds with mixed-ion channel pharmacology predicting TdP using hERG data alone may be challenging. A cell system that integrates such off-target effects may be expected to be more predictive. In this study we selected a diverse compound set with defined TdP risk and used the data from both our

hiPSC-CM model, as well as ion channel data, and employed a variety of statistical models/analyses to determine assay endpoints that predicted TdP risk.

In general, analyses using either single or multiple endpoints extracted from the hiPSC-CM model were shown to be highly predictive with the most predictive using four features from the model. The results were comparable with previous studies using smaller compound sets and lower throughput assay formats (Ando et al., 2017; Blinova et al., 2018; Kanda, Yamazaki, Osada, Yoshinaga & Sawada, 2018). The stem cell model was found to be more predictive than either ion channel data alone, O'Hara-Rudy modeling using ion channel data, or a combination of hiPSC-CM data and ion channel data.

Given the high-quality resolution of the data from the hiPSC-CM model, additional endpoints were examined to determine if the model had utility beyond predicting QTc and TdP. AP rise time is largely driven by the sodium current carried by Nav1.5, with Nav1.5 antagonists producing an increase in this parameter. An ROC cross validation analysis of AP rise time versus the ability of compounds to produce an increase in clinical QRS interval showed an excellent predictivity that was greater than that predicted by Nav1.5 patch clamp data, highlighting the value of this model in assessing QRS risk.

Finally, the ability of the model to define calcium channel (Cav1.2) block by compounds was examined. Due to the lack of a robust clinical PR interval data, the ECG endpoint most sensitive to calcium channel block, we instead looked at the ability of our model to predict Cav1.2 patch IC₅₀ values. We found that using the threshold concentration producing a decrease in the Yamamoto rate-corrected APD₉₀ value was an excellent predictor of Cav1.2 block, which is not

surprising given that calcium channel antagonists produce an atypical increase in beat rate in hIPSC-CM's (Zeng, Wang, Clouse, Lagrutta & Sannajust, 2019).

This study has certain limitations. The analysis relies on defining the risk of TdP for each compound, this can be challenging due to the low incidence rate of such arrhythmias, hence we only associated TdP risk in our study to compounds with a robust link to that endpoint. In addition, the predictivity of the model for certain endpoints may depend on a compound's ion channel selectivity. For a compound that is significantly more potent at one ion channel (i.e. > than a log selective), that activity will likely dominate in the model.

Overall, we describe an hIPSC-CM model that predicts clinic QTc, QRS and TdP risk and puts those risks into context with the expected free plasma exposure in the clinic. In addition, the high throughput format, and the ability to run in serum free conditions are major advantages when profiling early development compounds. The ability of the assay to be run over extended incubation times allows the detection of associated risks from compounds such as hERG traffic blockers or compounds that have slow on-rate kinetic, that would be missed using more conventional acute assays. The assay also replaces the need for ex vivo animal models, such as the Langendorff isolated heart model, that are routinely used to assess such risks.

In conclusion, the hIPSC-CM model described provides a convenient, cost effective, clinically translatable system that can predict multiple cardiac related risk endpoints. As such this model will play a key role in the early assessment of cardiac safety of development compounds.

5. Figures

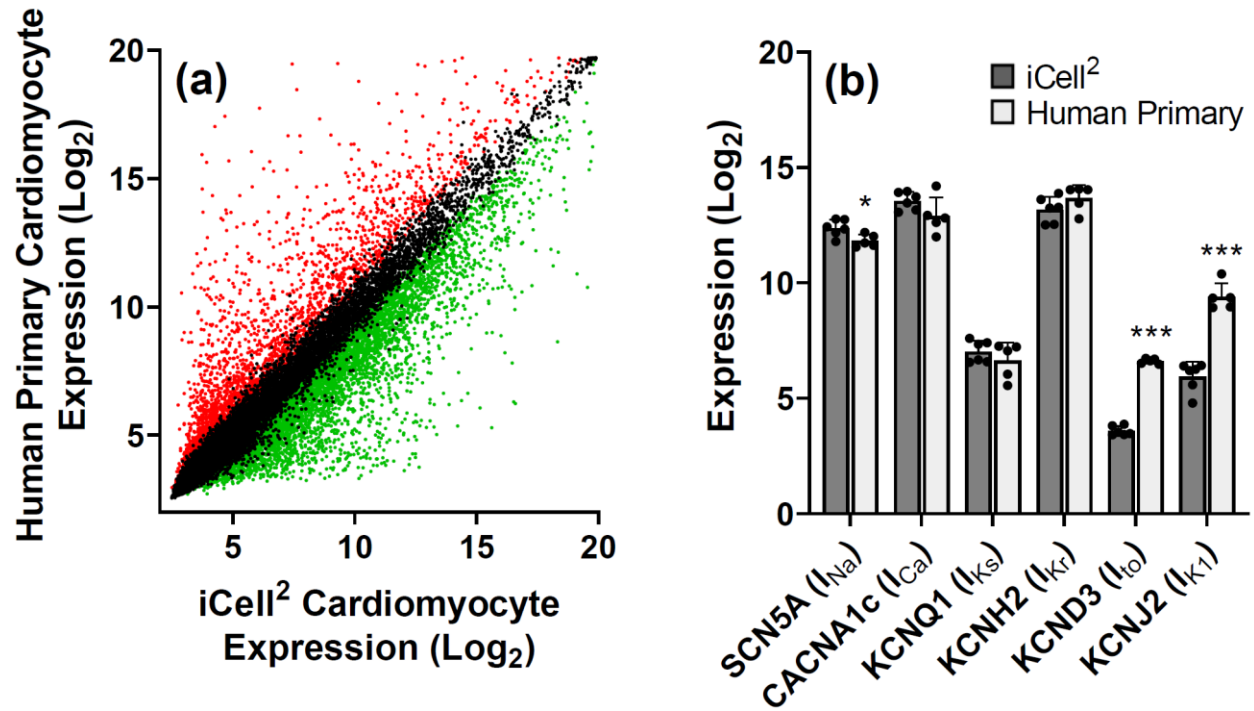


FIGURE 1 GeneChip expression analysis of iCell² hPSC cardiomyocytes and purified human primary ventricular cardiomyocytes. (a) Correlation of iCELL² hPSC cardiomyocytes ($n = 6$) and purified human primary ventricular cardiomyocytes ($n = 5$) transcript expression. A total of 48,234 transcripts were compared (significantly higher expression in iCell² cells highlighted in green ($P < .05$; F-Test); significantly lower expression in iCell² cell in red ($P < .05$, F-Test); no difference in expression in black). (b) Comparison of expression of key ion channels involved in cardiac action potential generation between iCell² cardiomyocytes ($n = 6$) and human primary cardiomyocytes ($n = 5$). Values are expressed as mean \pm SD. Statistically differences in channel transcript expression between iCell² and human primary cardiomyocytes are shown (* $P < .05$; *** $P < .001$; Welch's t -test).

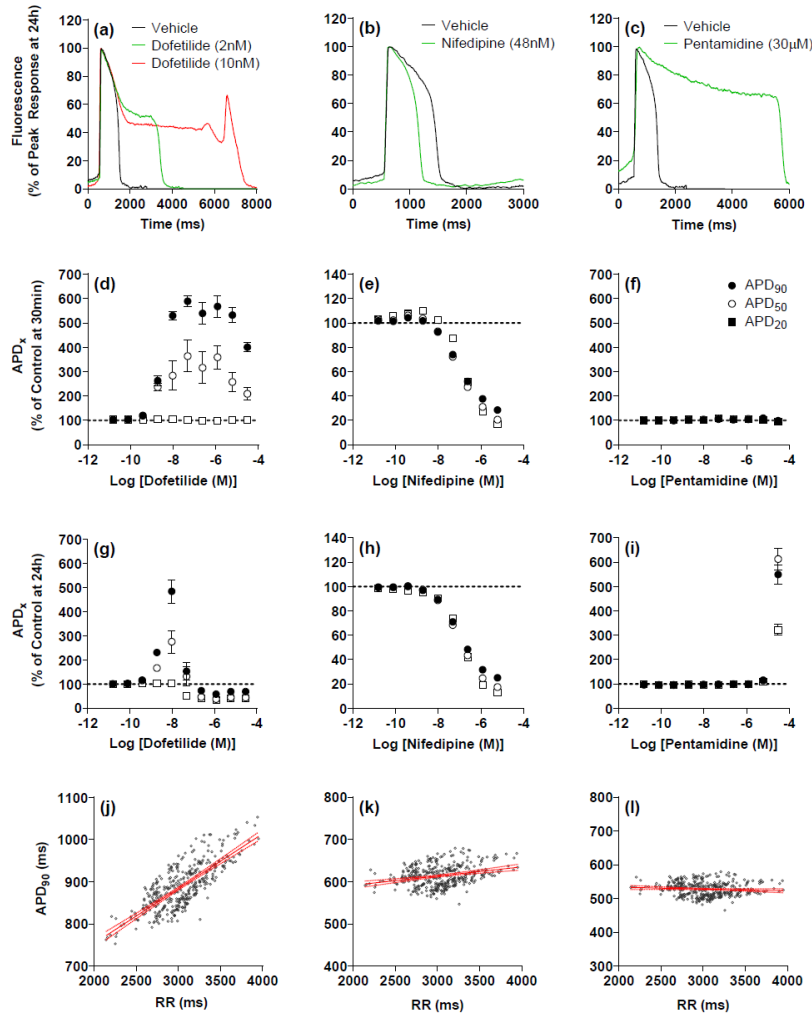


FIGURE 2 Effect of standard compounds on the iCell² hiPSC-CM action potential. (a-c) Example recording of action potentials following 24 h incubation with (a) the hERG blocker dofetilide, (b) the calcium channel blocker nifedipine, and (c) an inhibitor of hERG trafficking, pentamidine. Concentration response curves for the effects of standard compounds on action potential durations for 20% (APD₂₀), 50% (APD₅₀), and 90% (APD₉₀) recovery following an acute 30 min (d-f) or chronic 24 h (g-i) treatment. Data represent the mean \pm the standard error of the mean from a series of independent experiment (dofetilide ($n = 6$), nifedipine ($n = 3$) and pentamidine ($n = 6$)). Effect of action potential corrected for heart rate on APD₉₀ in vehicle treated iCell² hiPSC-CM's. (j) Uncorrected values (Slope = 0.130 ± 0.005), or values corrected

using the (k) Fridericia (Slope = 0.022 ± 0.004), or (l) Yamamoto (Slope = -0.005 ± 0.003) correction formulae. Data represent a total of 384 individual data points ($n = 24$ independent experiments, 16 data points per experiment). The optimal linear regression analysis fit is shown by the solid red line and the 95% confidence intervals of the fit represented by the dashed red lines.

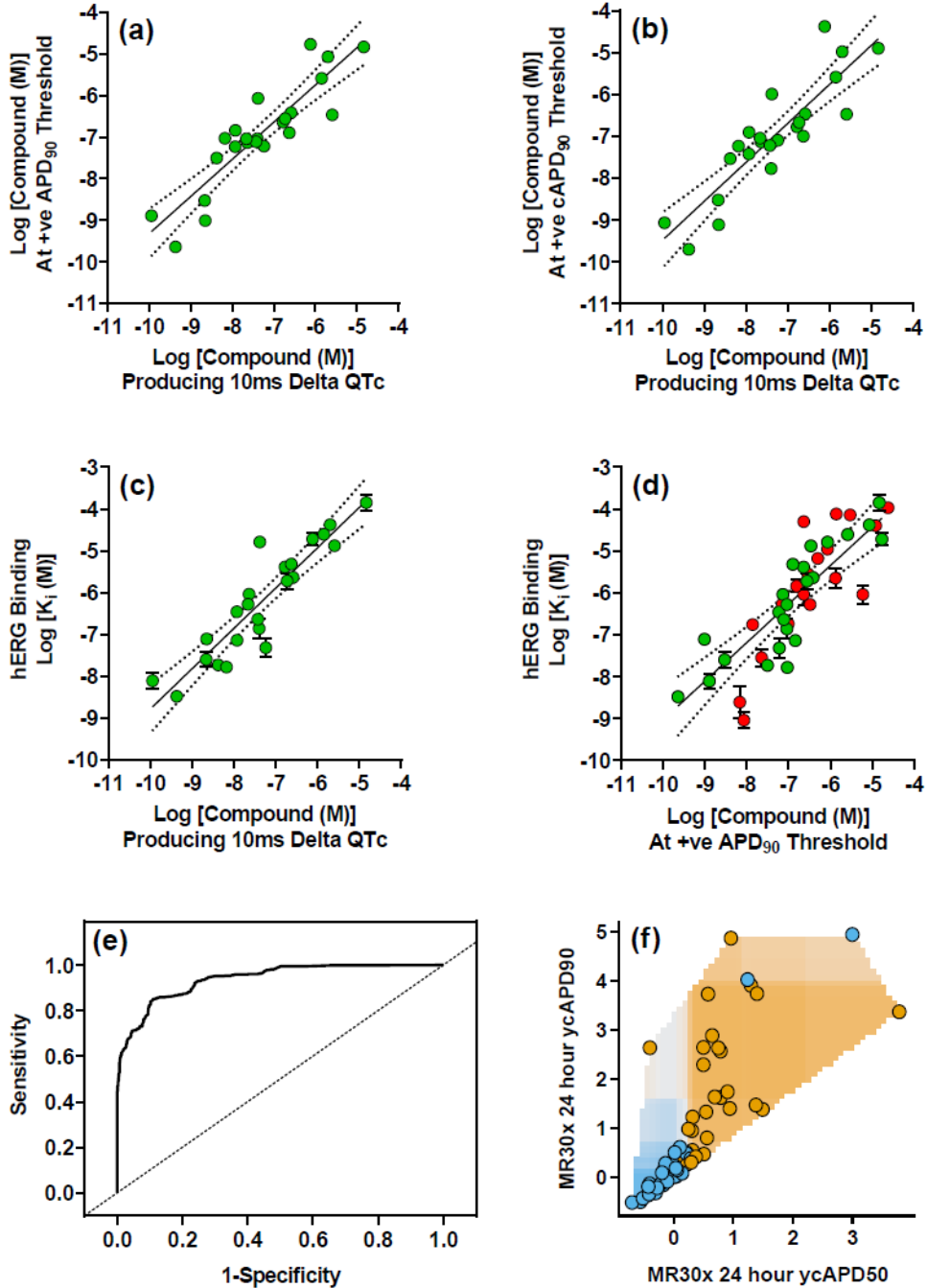


FIGURE 3 Correlation analysis of compounds concentrations required to produce a positive threshold change (defined as three times the standard deviation of control values) in hiPSC-CM (a) APD₉₀ and (b) Yamamoto-corrected APD₉₀ (cAPD₉₀) with the compound concentration required to produce a positive 10 ms change in QTc in the clinic. (c) Correlation of hERG

binding pK_i with compound concentration required to produce a 10 ms change in QTc in the clinic. For (a-c) data represent values from 23 compounds. (d) Correlation of hERG binding pK_i with compound concentration required to produce a threshold increase in APD₉₀. Data highlighted by green symbols represent compounds shown in (a-c). Data highlighted in red show correlation including an additional 19 test compounds where clinical QTc data were not available. Dotted lines represent the 95% CI of the linear fit. Data represent the mean. The standard deviation of the mean is shown for hERG binding data. (e-f) Example of a receiver operator curve analysis comparing TdP risk category versus maximum cAPD₉₀ change observed within a 10-fold concentration window of the EFTPC value for each compound following a 30 min incubation. (e) AUROC plot for the randomForest model trained using the MR30x values from the Yamamoto-corrected APD₉₀ and APD₅₀ endpoints from the 24 h time point, as well as the hill top values from the same curves ($n = 66$ compounds; AUROC value = 0.938). (f) Partial dependency plot. Orange shading indicates regions where the combination of features increases the probability of TdP+, while blue indicates a decrease in probability. The training data is represented as points colored by their observed TdP classification, with blue and orange representing TdP- and TdP+ compounds respectively.

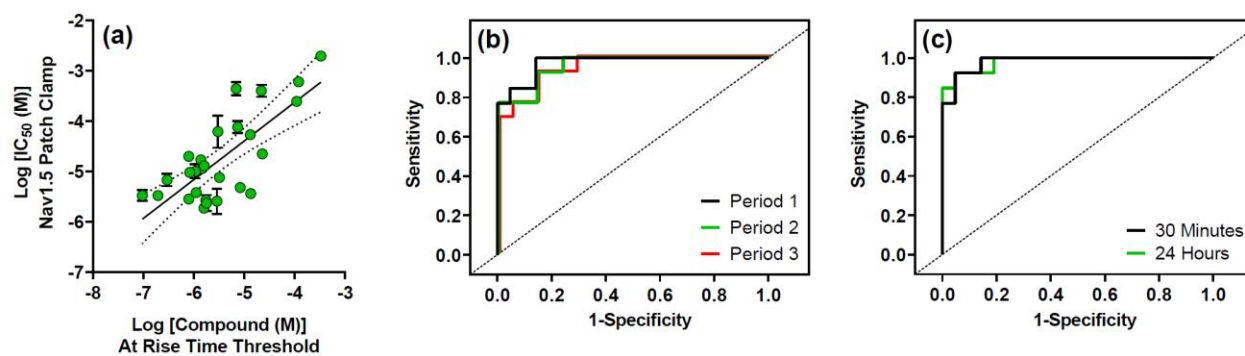


FIGURE 4 Comparison of hIPSC-CM action potential rise time, Nav1.5 channel inhibition with clinical QRS prolongation. (a) Correlation of compounds concentrations required to produce a positive threshold change (defined as three times the standard deviation of control values) in hIPSC-CM action potential rise time (24 h incubation time point) versus the IC₅₀ value generated in a Nav1.5 patch clamp assay (incubation period 1 only). (b) Receiver operator curve analysis of comparing Nav1.5 patch clamp assay IC₅₀ values (incubation period 1, 2 or 3) divided by the clinical free exposure versus the risk of an increase in QRS interval as defined by a published clinical observation ($n = 34$ compounds). (c) Receiver operator curve analysis of comparing ratio of rise time threshold concentration in hIPSC-CM assay (30 min or 24 h incubation) divided by the clinical free exposure versus the risk of an increase in QRS interval as defined by a published clinical observation ($n = 34$ compounds). A full analysis is shown in Table 6. Data represent the mean. The standard deviation of the mean is shown for patch clamp data.

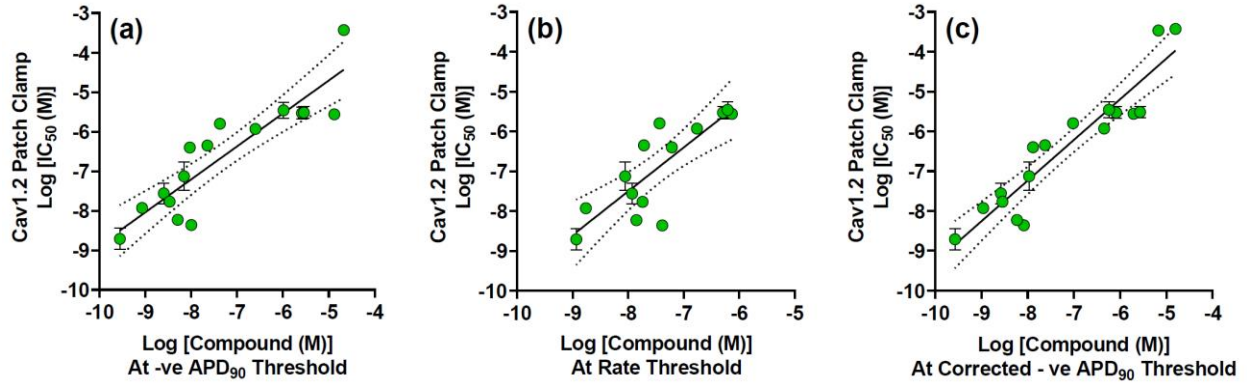


FIGURE 5 Effect of calcium channel antagonists on APD₉₀ in hIPSC-CM's. (a) Correlation of compounds concentrations required to produce a negative threshold change (defined as three times the standard deviation of control values) in hIPSC-CM APD₉₀ versus the IC₅₀ value generated in a Cav1.2 patch clamp assay (*n* = 16 compounds). (b) Correlation of compounds concentrations required to produce a positive threshold change (defined as three times the standard deviation of control values) in hIPSC-CM beat rate versus the IC₅₀ value generated in a Cav1.2 patch clamp assay (*n* = 14 compounds). (c) Correlation of compounds concentrations required to produce a negative threshold change (defined as three times the standard deviation of control values) in hIPSC-CM cAPD₉₀ (i.e. corrected for increases in beat rate) versus the IC₅₀ value generated in a Cav1.2 patch clamp assay (*n* = 17 compounds). Data represent the mean. The standard deviation of the mean is shown for patch clamp data.

Table 1. Effect of compounds on iPSC cardiomyocyte APD₉₀, hERG channel binding and clinical QTc interval

Compound	Threshold Drug Concentration for hiPSC-CM Endpoint Log [Concentration (nM)]				hERG Binding	Clinical QTc
	APD ₉₀ (30 min)	APD ₉₀ (24 h)	cAPD ₉₀ (30 min)	cAPD ₉₀ (24 h)	pK _i ± SD (n)	Free Exposure Producing 10ms Change Log [Concentration (nM)]
Azimilide	-6.57	-7.23	-6.59	-7.42	-6.46 ± 0.02 (3)	-7.93
Bepidil	-7.24	-6.84	-7.57	-6.90	-7.14 ± 0.04 (6)	-7.93
Cisapride	-8.14	-7.50	-8.39	-7.54	-7.73 ± 0.05 (6)	-8.38
Citalopram	-6.47	-6.64	-6.54	-6.78	-5.39 ± 0.04 (3)	-6.78
Dofetilide	-9.40	-9.65	-9.55	-9.70	-8.48 ± 0.08 (6)	-9.37
Droperidol	-7.95	-7.04	-8.14	-7.77	-6.86 ± 0.24 (6)	-7.40
E4031	-8.65	-9.01	-8.87	-9.12	-7.11 ± 0.04 (3)	-8.65
Halofantrine	-6.46	-7.22	-6.55	-7.10	-7.52 ± 0.12 (3)	-7.24
Ibutilide	-9.30	-8.89	-9.41	-9.07	-8.11 ± 0.18 (6)	-9.95
Lamotrigine	> -4.52	> -4.52	> -4.52	> -4.52	> -4.10 (3)	> -4.61
Levocetirizine	-4.65	-4.92	-4.64	-4.81	-4.40 ± 0.07 (3)	> -6.88
Levofloxacin	-4.70	-4.72	-4.70	-4.72	> -4.10 (3)	> -5.54
Mesoridazine	-6.40	-6.90	-6.47	-7.00	-5.32 ± 0.04 (3)	-6.63
Moxifloxacin	-4.54	-5.07	-4.53	-4.98	-4.38 ± 0.11 (3)	-5.70
Odansetron	-6.40	-6.42	-6.43	-6.47	-5.64 ± 0.10 (6)	-6.59
Paliperidone	-6.90	-6.81	-6.95	-6.99	-5.84 ± 0.15 (6)	> -7.52
Procainamide	-5.37	-4.83	-5.22	-4.90	-3.85 ± 0.19 (4)	-4.83
Quinidine	-6.78	-6.56	-6.86	-6.67	-5.72 ± 0.19 (6)	-6.73
Quinine	-6.78	-6.47	-6.74	-6.48	-4.88 ± 0.14 (3)	-5.59
Ranolazine	-5.86	-5.59	-6.24	-5.59	-4.61 ± 0.02 (3)	-5.85
Ribociclib	-5.82	-6.07	-5.60	-5.99	-4.73 ± 0.04 (3)	-7.38
Risperidone	-7.35	-7.15	-7.36	-7.25	-6.27 ± 0.09 (6)	> -7.44
Sotalol	-5.57	-4.77	-5.46	-4.38	-4.72 ± 0.15 (6)	-6.12
Terfenadine	-7.86	-7.03	-8.46	-7.24	-7.78 ± 0.14 (6)	-8.18
Terodiline	-6.93	-7.14	-7.02	-7.14	-6.04 ± 0.08 (3)	-7.64
Thioridazine	-6.72	-7.11	-6.74	-7.22	-6.64 ± 0.08 (3)	-7.43
Tolterodine	-8.41	-8.53	-8.47	-8.52	-7.60 ± 0.18 (3)	-8.67
Vandetanib	-6.73	-7.04	-6.52	-7.05	-6.28 ± 0.03 (3)	-7.66
Verapamil	> -4.52	> -4.52	> -4.52	> -4.52	-5.94 ± 0.32 (6)	> -7.43

Table 2. Summary statistics for correlation of hIPSC-CM APD₉₀ values and hERG binding to clinical QTc

Endpoint Comparison			Spearman Rank Correlation (ρ Value)		Pearson Correlation (r^2 Value)	
hIPSC-CM Assay Incubation Time	X-Axis	Y-Axis	Non-Censored Data	All Data	Non-Censored Data	Correlation Equation
30 min	QTc	APD ₉₀	0.799 (23)	0.767 (29)	0.762 (23)	$Y = 0.86X - 0.64$
30 min	QTc	cAPD ₉₀	0.841 (23)	0.795 (29)	0.737 (23)	$Y = 0.92X - 0.35$
30 min	APD ₉₀	hERG Binding	0.785 (23)	0.807 (29)	0.786 (23)	$Y = 0.95X + 0.39$
30 min	cAPD ₉₀	hERG Binding	0.823 (23)	0.838 (29)	0.799 (23)	$Y = 0.89X + 0.04$
24 h	QTc	APD ₉₀	0.882 (23)	0.822 (29)	0.800 (23)	$Y = 0.89X - 0.39$
24 h	QTc	cAPD ₉₀	0.893 (23)	0.818 (29)	0.776 (23)	$Y = 0.93X - 0.17$
24 h	APD ₉₀	hERG Binding	0.842 (23)	0.860 (29)	0.757 (23)	$Y = 0.92X + 0.18$
24 h	cAPD ₉₀	hERG Binding	0.847 (23)	0.861 (29)	0.755 (23)	$Y = 0.87X - 0.13$
-	QTc	hERG Binding (pK _i)	0.883 (23)	0.889 (29)	0.832 (23)	$Y = 0.96X + 0.85$

$P < 0.0001$ for all correlations shown. Number of compounds included in correlation shown in parenthesis. cAPD₉₀; Yamamoto corrected APD₉₀ values.

Table 3. Overview of Torsades de Pointes predictive modeling analysis

Assay Format	Inputs	Features	Method	AUROC	MCC	TP	TN	FP	FN
Stem Cell	Multiple	modl_tp_24h_ycAPD50 modl_tp_24h_ycAPD90 MR30x_24h_ycAPD50 MR30x_24h_ycAPD90	randomForest	0.938	0.736	24.70	32.70	4.30	4.30
Stem Cell/ Ion Channel	Multiple	modl_tp_24h_ycAPD50 modl_tp_24h_ycAPD90 MR30x_24h_ycAPD50 MR30x_24h_ycAPD90 gherg / gcav / gnvp	randomForest	0.930	0.734	24.80	32.55	4.45	4.20
Stem Cell	Single	MR10x_0.5h_ycAPD90	Logistic Regression	0.917	0.676	21.30	34.10	2.90	7.70
Ion Channel/ O'Hara Model	Multiple	logconcM_10ms_margin	Logistic Regression	0.845	0.627	23.90	29.85	7.15	5.10
Ion Channel	Multiple	gherg / gcav / gnvp	randomForest	0.819	0.496	20.35	29.30	7.70	8.65

All data represent 20 times 5-fold cross validation analyses. AUROC: area under receiver operator curve; MCC: Matthews correlation coefficient; TP: true positive; TN: true negative; FP: false positive; FN: false negative; MR10x or MR30x: maximum response within a 10x or 30x margin of the EFTPC; modl_tp: maximum asymptote of curve fit at any concentration; ycAPD50 or ycAPD90: Yamamoto-corrected action potential duration 50 or 90; 0.5h or 24h: 0.5 h or 24 h assay incubation time; gherg / gcav / gnvp: calculated fractional block of hERG / Cav1.2 / Nav1.5 (peak) at a 30x multiple of the EFTPC; logconcM_10ms_margin: calculated concentration of compound required to produce a 10 ms increase in action potential duration using the output of O'Hara-Rudy modeling of ion channel data (O'Hara et al., 2011).

Table 4. Effect of compounds on clinical QRS interval, hIPSC action potential rise time and Nav1.5 patch clamp

Compound	Clinical Data		hIPSC-CM Data	Nav1.5 Patch Clamp Data		
	Clinical QRS Prolongation Observed	Clinical Free Exposure (μM)	Rise Time Threshold Concentration At 24 h (μM)	Period 1 IC ₅₀ (μM)	Period 2 IC ₅₀ (μM)	Period 3 IC ₅₀ (μM)
Amitriptyline	Yes	0.17	1.6	1.8	1.1	0.9
Astemizole	No	0.0036	0.1	3.3	2.0	1.5
Bepridil	No	0.03	3.2	7.5	3.3	2.3
Bupivacaine	Yes	0.21	8.3	4.8	3.8	3.1
Carbamazepine	Yes	62.72	119.0	602.6	446.7	398.1
Chlorpromazine	No	0.04	13.4*	3.6	2.0	1.4
Cisapride	No	0.003	1.5	11.4	6.2	4.6
Citalopram	Yes	1.20	7.9	46.9	39.6	35.7
Clomipramine	No	0.02	8.9*	2.6	1.9	1.4
Clozapine	No	0.07	13.4*	17.5	13.3	9.0
Desipramine	Yes	0.12	1.7	2.7	1.6	1.4
Disopyramide	Yes	1.82	21.9	396.0	288.3	189.4
Domperidone	No	0.02	1.1	10.0	3.7	3.3
Flecainide	Yes	0.12	1.4	16.9	12.0	10.6
Imipramine	Yes	0.04	2.3	2.6	1.1	1.1
Lamotrigine	Yes	26.01	6.9	433.2	332.3	240.9
Loratadine	No	0.0005	3.0	44.7	31.4	20.8
Maprotiline	Yes	0.06	1.8	2.3	1.5	1.2
Mesoridazine	Yes	2.07	1.6	12.9	9.1	8.0
Mexiletine	Yes	1.03	20.4	95.5	49.4	41.8
Moxifloxacin	No	2.84	>300.0	>1000.0	>1000.0	>831.8
Nicardipine	No	0.01	0.7*	9.6	4.9	3.3
Nortriptyline	Yes	0.03	0.8	1.8	1.1	0.9
Pimozide	No	0.001	0.2	3.3	1.4	1.2
Procainamide	Yes	26.01	329.0	1957.1	1512.6	1238.9
Propafenone	Yes	0.15	0.8	2.8	1.7	1.3
Quinidine	Yes	1.08	9.6	19.8	14.4	13.3
Quinine	Yes	0.81	13.1	53.2	45.7	34.2
Risperidone	Yes	0.31	7.5	76.6	54.1	45.0
Ropivacaine	Yes	2.51	22.9	22.6	17.1	13.0
Sertindole	No	0.002	0.3	6.8	2.7	1.7
Terfenadine	No	0.009	2.7*	3.3	2.0	1.5
Thioridazine	Yes	0.82	1.1	3.8	2.1	1.5
Venlafaxine	Yes	22.71	108.4	245.5	177.4	160.1

*Geometric mean concentration determined for cells transitioning to quiescence without increase in AP rise time

Table 5. Summary statistics for receiver-operator curve analysis of hIPSC-CM rise time, Nav1.5 patch clamp and clinical QRS data

Assay Format	Incubation	AUROC Value (95% CI)	Sensitivity Value (95% CI)	Specificity Value (95% CI)	Cut Point Value	<i>n</i> Value
hIPSC-CM	30 min	0.982 (0.949, 1.014)	0.922 (0.640, 0.998)	0.952 (0.762, 0.999)	33.0	34
hIPSC-CM	24 h	0.982 (0.948, 1.016)	0.922 (0.640, 0.998)	0.952 (0.762, 0.999)	56.4	34
Nav1.5 Patch	Period 1	0.974 (0.934, 1.015)	1.000 (0.753, 1.000)	0.857 (0.637, 0.970)	95.0	34
Nav1.5 Patch	Period 2	0.960 (0.904, 1.016)	0.923 (0.640, 0.998)	0.857 (0.637, 0.970)	93.1	34
Nav1.5 Patch	Period 3	0.953 (0.890, 1.015)	0.923 (0.640, 0.998)	0.857 (0.637, 0.970)	70.1	34

95% CI; 95% confidence intervals. *n* value represents the number of compounds included in the analysis

6. Acknowledgments

The authors would like to thank Todd Wisialowski and Gregg Cappon for their critical review of this manuscript and their insightful suggestions.

7. Author Contributions

S.J. conceived and designed the study. P.K., L.F., A.B., T.L. and S.J. performed the experimental procedures. P.K. L.F., A.B., T.L., D.L. and S.J. analyzed the data. D.Li performed the statistical analysis and E.W. performed the modeling analysis. P.K, D.L., D.Li, D.J.M, P.S., E.W. and S.J. drafted the manuscript.

8. Conflict of Interest

The authors declare no conflicts of interest.

9. Declaration of Transparency and Scientific Rigour

This Declaration acknowledges that this paper adheres to the principles for transparent reporting and scientific rigour of preclinical research as stated in the BJP guidelines for Design & Analysis and as recommended by funding agencies, publishers and other organizations engaged with supporting research.

10. Data Availability Statement

Additional supporting data may be found online in the Supporting Information section.

11. References.

Akaike H (1998). Information Theory and an Extension of the Maximum Likelihood Principle. In Selected Papers of Hirotugu Akaike. eds Parzen E., Tanabe K., & Kitagawa G. Springer, New York, NY, pp 199-213.

Alexander SPH, Mathie A, Peters JA, Veale EL, Striessnig J, Kelly E, *et al.* (2019). THE CONCISE GUIDE TO PHARMACOLOGY 2019/20: Ion channels. *Br J Pharmacol* 176 Suppl 1: S142-S228.

Ando H, Yoshinaga T, Yamamoto W, Asakura K, Uda T, Taniguchi T, *et al.* (2017). A new paradigm for drug-induced torsadogenic risk assessment using human iPS cell-derived cardiomyocytes. *J Pharmacol Toxicol Methods* 84: 111-127.

Anon (2020). E14 and S7B clinical and nonclinical evaluation of QT/QTc interval prolongation and proarrhythmic potential - Questions and answers. Retrieved from <https://www.fda.gov/regulatory-information/search-fda-guidance-documents/e14-and-s7b-clinical-and-nonclinical-evaluation-qtqtc-interval-prolongation-and-proarrhythmic>.

Bazett HC (1920). An analysis of the time-relations of the electrocardiograms. *Heart* 7: 353-370.

Blinova K, Dang Q, Millard D, Smith G, Pierson J, Guo L, *et al.* (2018). International Multisite Study of Human-Induced Pluripotent Stem Cell-Derived Cardiomyocytes for Drug Proarrhythmic Potential Assessment. *Cell Rep* 24: 3582-3592.

Colatsky T, Fermini B, Gintant G, Pierson JB, Sager P, Sekino Y, *et al.* (2016). The Comprehensive in Vitro Proarrhythmia Assay (CiPA) initiative - Update on progress. *J Pharmacol Toxicol Methods* 81: 15-20.

Curtis MJ, Alexander S, Cirino G, Docherty JR, George CH, Giembycz MA, *et al.* (2018). Experimental design and analysis and their reporting II: updated and simplified guidance for authors and peer reviewers. *Br J Pharmacol* 175: 987-993.

Fermini B, Hancox JC, Abi-Gerges N, Bridgland-Taylor M, Chaudhary KW, Colatsky T, *et al.* (2016). A New Perspective in the Field of Cardiac Safety Testing through the Comprehensive In Vitro Proarrhythmia Assay Paradigm. *J Biomol Screen* 21: 1-11.

Ficker E, Dennis AT, Wang L, & Brown AM (2003). Role of the cytosolic chaperones Hsp70 and Hsp90 in maturation of the cardiac potassium channel HERG. *Circ Res* 92: e87-100.

Filer DL, Kothiya P, Setzer RW, Judson RS, & Martin MT (2017). tcpl: the ToxCast pipeline for high-throughput screening data. *Bioinformatics* 33: 618-620.

Food, & Drug Administration HHS (2005). International Conference on Harmonisation; guidance on S7B Nonclinical Evaluation of the Potential for Delayed Ventricular Repolarization (QT Interval Prolongation) by Human Pharmaceuticals; availability. Notice. Fed Regist 70: 61133-61134.

Fridericia LS (1920). Die systolendauer im elektrokardiogramm bei normalen menschen und bei herzkranken. Acta Med Scand 53: 469-486.

Friedman J, Hastie T, & Tibshirani R (2010). Regularization Paths for Generalized Linear Models via Coordinate Descent. J Stat Softw 33: 1-22.

Garg P, Garg V, Shrestha R, Sanguinetti MC, Kamp TJ, & Wu JC (2018). Human Induced Pluripotent Stem Cell-Derived Cardiomyocytes as Models for Cardiac Channelopathies: A Primer for Non-Electrophysiologists. Circ Res 123: 224-243.

Gintant G, Fermini B, Stockbridge N, & Strauss D (2017). The Evolving Roles of Human iPSC-Derived Cardiomyocytes in Drug Safety and Discovery. Cell Stem Cell 21: 14-17.

Gintant G, Kaushik EP, Feaster T, Stoelzle-Feix S, Kanda Y, Osada T, *et al.* (2020). Repolarization studies using human stem cell-derived cardiomyocytes: Validation studies and best practice recommendations. Regul Toxicol Pharmacol 117: 104756.

Gintant G, & Traebert M (2020). The roles of human induced pluripotent stem cell-derived cardiomyocytes in drug discovery: managing in vitro safety study expectations. Expert Opin Drug Discov 15: 719-729.

Goksuluk D, Krokmaz S, Zararsiz G, & Karaagaoglu AE (2016). An Interactive Web-tool for ROC Curve Analysis Using R Language Environment. The R Journal 8: 213-230.

Greenwell BM (2017). pdp: An R Package for Constructing Partial Dependence Plots. The R Journal 9: 421-436.

Harding SD, Sharman JL, Faccenda E, Southan C, Pawson AJ, Ireland S, *et al.* (2018). The IUPHAR/BPS Guide to PHARMACOLOGY in 2018: updates and expansion to encompass the new guide to IMMUNOPHARMACOLOGY. Nucleic Acids Res 46: D1091-D1106.

Harmer AR, Valentin JP, & Pollard CE (2011). On the relationship between block of the cardiac Na(+) channel and drug-induced prolongation of the QRS complex. Br J Pharmacol 164: 260-273.

Ivashchenko CY, Pipes GC, Lozinskaya IM, Lin Z, Xiaoping X, Needle S, *et al.* (2013). Human-induced pluripotent stem cell-derived cardiomyocytes exhibit temporal changes in phenotype. *Am J Physiol Heart Circ Physiol* 305: H913-922.

Johannesen L, Vicente J, Mason JW, Sanabria C, Waite-Labott K, Hong M, *et al.* (2014). Differentiating drug-induced multichannel block on the electrocardiogram: randomized study of dofetilide, quinidine, ranolazine, and verapamil. *Clin Pharmacol Ther* 96: 549-558.

Johnson SG (2017). The NLOpt nonlinear-optimization package. Retrieved from <http://github.com/stevengi/nlopt>.

Kanda Y, Yamazaki D, Osada T, Yoshinaga T, & Sawada K (2018). Development of torsadogenic risk assessment using human induced pluripotent stem cell-derived cardiomyocytes: Japan iPS Cardiac Safety Assessment (JiCSA) update. *J Pharmacol Sci* 138: 233-239.

Kuhn M (2020). caret: Classification and regression training. Retrieved from <https://CRAN.R-project.org/package=caret>.

Lancaster MC, & Sobie EA (2016). Improved Prediction of Drug-Induced Torsades de Pointes Through Simulations of Dynamics and Machine Learning Algorithms. *Clin Pharmacol Ther* 100: 371-379.

Lee HA, Hyun SA, Park SG, Kim KS, & Kim SJ (2016). Comparison of electrophysiological effects of calcium channel blockers on cardiac repolarization. *Korean J Physiol Pharmacol* 20: 119-127.

Liaw A, & Wiener M (2002). Classification and Regression by randomForest. *R News* 2: 18-22.

Ma J, Guo L, Fiene SJ, Anson BD, Thomson JA, Kamp TJ, *et al.* (2011). High purity human-induced pluripotent stem cell-derived cardiomyocytes: electrophysiological properties of action potentials and ionic currents. *Am J Physiol Heart Circ Physiol* 301: H2006-2017.

Matthews BW (1975). Comparison of the predicted and observed secondary structure of T4 phage lysozyme. *Biochim Biophys Acta* 405: 442-451.

Millard D, Dang Q, Shi H, Zhang X, Strock C, Kraushaar U, *et al.* (2018). Cross-Site Reliability of Human Induced Pluripotent stem cell-derived Cardiomyocyte Based Safety Assays Using Microelectrode Arrays: Results from a Blinded CiPA Pilot Study. *Toxicol Sci* 164: 550-562.

O'Hara T, Virag L, Varro A, & Rudy Y (2011). Simulation of the undiseased human cardiac ventricular action potential: model formulation and experimental validation. *PLoS Comput Biol* 7: e1002061.

Page G, Ratchada P, Miron Y, Steiner G, Ghetti A, Miller PE, *et al.* (2016). Human ex-vivo action potential model for pro-arrhythmia risk assessment. *J Pharmacol Toxicol Methods* 81: 183-195.

Perez-Hernandez M, Matamoros M, Alfayate S, Nieto-Marin P, Utrilla RG, Tinaquero D, *et al.* (2018). Brugada syndrome trafficking-defective Nav1.5 channels can trap cardiac Kir2.1/2.2 channels. *JCI Insight* 3.

Pfeiffer-Kaushik ER, Smith GL, Cai B, Dempsey GT, Hortigon-Vinagre MP, Zamora V, *et al.* (2019). Electrophysiological characterization of drug response in hSC-derived cardiomyocytes using voltage-sensitive optical platforms. *J Pharmacol Toxicol Methods* 99: 106612.

Powell MJD (2009). The BOBYQA algorithm for bound constrained optimization without derivatives. Retrieved from http://www.damtp.cam.ac.uk/user/na/NA_papers/NA2009_06.pdf.

R-Project (2019). R: A language and environment for statistical computing. Retrieved from <https://www.R-project.org/>.

Ribeiro AJS, Guth BD, Engwall M, Eldridge S, Foley CM, Guo L, *et al.* (2019). Considerations for an In Vitro, Cell-Based Testing Platform for Detection of Drug-Induced Inotropic Effects in Early Drug Development. Part 2: Designing and Fabricating Microsystems for Assaying Cardiac Contractility With Physiological Relevance Using Human iPSC-Cardiomyocytes. *Front Pharmacol* 10: 934.

Roden DM (2004). Drug-induced prolongation of the QT interval. *N Engl J Med* 350: 1013-1022.

Saxena P, Hortigon-Vinagre MP, Beyl S, Baburin I, Andranovits S, Iqbal SM, *et al.* (2017). Correlation between human ether-a-go-go-related gene channel inhibition and action potential prolongation. *Br J Pharmacol* 174: 3081-3093.

Spearman C (1987). The proof and measurement of association between two things. By C. Spearman, 1904. *Am J Psychol* 100: 441-471.

Tan HL, Bezzina CR, Smits JP, Verkerk AO, & Wilde AA (2003). Genetic control of sodium channel function. *Cardiovasc Res* 57: 961-973.

Therneau T, & Atkinson B (2019). Rpart: Recursive partitioning and regression trees. Retrieved from <https://CRAN.R-project.org/package=rpart>.

Welch BL (1947). The generalisation of student's problems when several different population variances are involved. *Biometrika* 34: 28-35.

Yamamoto W, Asakura K, Ando H, Taniguchi T, Ojima A, Uda T, *et al.* (2016). Electrophysiological Characteristics of Human iPSC-Derived Cardiomyocytes for the Assessment of Drug-Induced Proarrhythmic Potential. *PLoS One* 11: e0167348.

Zeng H, Wang J, Clouse H, Lagrutta A, & Sannajust F (2019). Resolving the Reversed Rate Effect of Calcium Channel Blockers on Human-Induced Pluripotent Stem Cell-Derived Cardiomyocytes and the Impact on In Vitro Cardiac Safety Evaluation. *Toxicol Sci* 167: 573-580.

Zhao Z, Lan H, El-Battrawy I, Li X, Buljubasic F, Sattler K, *et al.* (2018). Ion Channel Expression and Characterization in Human Induced Pluripotent Stem Cell-Derived Cardiomyocytes. *Stem Cells Int* 2018: 6067096.

Zhu WZ, Santana LF, & Laflamme MA (2009). Local control of excitation-contraction coupling in human embryonic stem cell-derived cardiomyocytes. *PLoS One* 4: e5407.

12. Supplementary Data

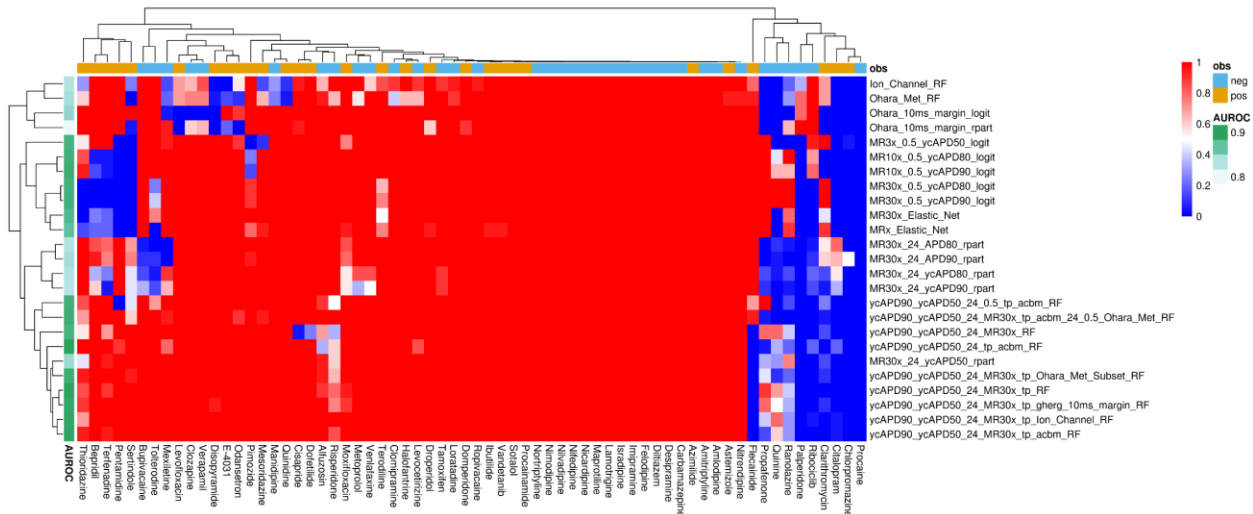


FIGURE S1 Summary of Effect Modeling results. Each row is a different model with indication of the features and algorithm used. Columns represent each compound in the training set. The green bar on the left indicates the AUROC (light to dark shade represents lower to higher AUROC values) while the top blue/orange indicates TdP-/TdP+, respectively. Cells colored red were correctly predicted in the respective models, while cells colored blue were incorrectly predicted.

Key to Terms for Figure S1:

Ion_Channel: Direct ion channel block values at 30x EFTPC

Ohara_Met: Metrics from the O'Hara-Rudy Carditomyocyte model at 30x EFTPC

Ohara_10ms_margin: The Exposure margin needed for a 10ms increase in APD90 in the O'Hara Rudy model

MR3x/MR10x/MR30x: Maximum response at 3x/10x/30x EFTPC in the stem cell assay

0.5/24: Readout at 0.5 or 24 hours after exposure in the stem cell assay

ycAPD50/ycAPD80/ycAPD90: Yamamoto-corrected APD50/APD80/APD90

tp: Asymptotic top fitted in the hill model for the stem cell assay endpoint

acbm: The margin between EFTPC and the activity concentration at baseline (3 times baseline median absolute deviation).

RF/logit/Elastic_Net/rpart: Machine learning algorithm used; randomForest/Logistic

Regression/Elastic Net/Recursive Partitioning and Regression Trees

Figure Results/Discussion For Figure S1: The modeling results were explored for each model and compound. The first 4 rows are models trained on various ion channel inhibition features alone. These show a different pattern than the stem cell based models, with more compounds incorrectly predicted. The logistic regression and elastic net models (rows 5-11) incorrectly predict a few compounds that the other models handle correctly (first five columns), yet the AUROC values are still fairly high. The optimal model, a randomForest model trained on the Yamamoto-corrected APD90 and APD50 MR30x and hill top parameters, is shown on row 22 (Labelled as: ycAPD90_ycAPD50_24_MR30x_tp_RF). Since the compounds incorrectly predicted in this model are consistently mispredicted in the other models, there is little reason to think that adding more features will improve the predictive performance. Indeed, rows 21 and 23-25 which add ion channel or other stem cell features to this model have a similar prediction pattern with similar to slightly reduced AUROC/MCC values. Moreover, this combined with the high AUROC and MCC values for this model suggest there is little to be gained by increasing model complexity.

Table S1. Primary ventricular cardiomyocyte donor characteristics

Donor	Age	Sex	Ethnicity	BMI	Cause of Death
1	46	F	Caucasian	30.5	CVA/ICH/Stroke
2	46	F	Hispanic	25.9	CVA/ICH/Stroke
3	53	F	Caucasian	28.0	CVA/ICH/Stroke
4	47	M	Hispanic	29.8	CVA/ICH/Stroke
5	55	M	Caucasian	22.9	CVA/ICH/Stroke

F, Female; M, Male; BMI, Body Mass Index; CVA, Cerebrovascular Accident; ICH, Intracranial heamorrhage.

Table S2. References for clinical QTc

Compound	Clinical QTc	
	^a Free Exposure Producing 10ms Change Log [Concentration (nM)]	References
Azimilide	-7.93	(Corey, Agnew, Brum, Parekh, Valentine & Williams, 1999; Phillips, 2001)
Bepidil	-7.93	(Duchene-Marullaz, Kantelip & Trolese, 1983)
Cisapride	-8.38	(Chain, Dubois, Danhof, Sturkenboom, Della Pasqua & Cardiovascular Safety Project Team, 2013)
Citalopram	-6.78	(Friberg, Isbister & Duffull, 2006)
Dofetilide	-9.37	(Darpo et al., 2015; Johannesen et al., 2014; Jonker, Kenna, Leishman, Wallis, Milligan & Jonsson, 2005; Sedgwick, Rasmussen, Walker & Cobbe, 1991)
Droperidol	-7.40	(Charbit, Alvarez, Dasque, Abe, Demolis & Funck-Brentano, 2008)
E4031	-8.65	(Katritsis et al., 1997)
Halofantrine	-7.24	(Abemethy et al., 2001b)
Ibutilide	-9.95	(Tisdale et al., 2012)
Lamotrigine	> -4.61	(Dixon et al., 2008)
Levocetirizine	> -6.88	(Darpo et al., 2015)
Levofloxacin	> -5.54	(Noel, 2003)
Mesoridazine	-6.63	(Salih, Thanacoody, McKay & Thomas, 2007)
Moxifloxacin	-5.70	(Chain, Dubois, Danhof, Sturkenboom, Della Pasqua & Cardiovascular Safety Project Team, 2013; Darpo et al., 2015; Dixon et al., 2008; Hulhoven, Rosillon, Letiexhe, Meeus, Daoust & Stockis, 2007; Noel, 2003) ¹ FDA Documents
Odansetron	-6.59	(Darpo et al., 2015)
Paliperidone	> -7.52	(Hough, Natarajan, Vandebosch, Rossenu, Kramer & Eerdeken, 2011)
Procinamide	-4.83	(Platia, Weisfeldt & Franz, 1988; Reiter, Higgins, Payne & Mann, 1986)
Quinidine	-6.73	(Benton, Sale, Flockhart & Woosley, 2000; Johannesen et al., 2014)
Quinine	-5.59	(Darpo et al., 2015)
Ranolazine	-5.85	(Johannesen et al., 2014)
Ribociclib	-7.38	² FDA Documents
Risperidone	> -7.44	(Harigan et al., 2004)
Sotalol	-6.12	(Chain, Dubois, Danhof, Sturkenboom, Della Pasqua & Cardiovascular Safety Project Team, 2013; Funck-Brentano, 1993; Uematsu, Kanamaru & Nakashima, 1994)
Terfenadine	-8.18	(Abemethy et al., 2001a; Honig, Wortham, Zamani, Dp, Mullin & Cantilena, 1993)
Terodiline	-7.64	(Thomas et al., 1995)
Thioridazine	-7.43	(Salih, Thanacoody, McKay & Thomas, 2007)
Tolterodine	-8.67	(Sweeney, Gastonguay, Benincosa, Cronenberger, Glue & Malhotra, 2010)
Vandetanib	-7.66	³ FDA Documents
Verapamil	> -7.43	(Johannesen et al., 2014)

^aFree exposure concentration producing a 10ms change in clinical QTc was calculated from a single fit combining all available data. See methods for more detail regarding curve fitting methodology.

References

- Abemethy DR, Barbey JT, Franc J, Brown KS, Feinera I, Ford N, *et al.* (2001a). Loratadine and terfenadine interaction with nefazodone: Both antihistamines are associated with QTc prolongation. *Clin Pharmacol Ther* 69: 96-103.
- Abemethy DR, Wesche DL, Barbey JT, Ohrt C, Mohanty S, Pezzullo JC, *et al.* (2001b). Stereoselective halofantrine disposition and effect: concentration-related QTc prolongation. *Br J Clin Pharmacol* 51: 231-237.
- Benton RE, Sale M, Flockhart DA, & Woosley RL (2000). Greater quinidine-induced QTc interval prolongation in women. *Clin Pharmacol Ther* 67: 413-418.
- Chain ASY, Dubois VFS, Danhof M, Sturkenboom MCJM, Della Pasqua O, & Cardiovascular Safety Project Team TIPPP (2013). Identifying the translational gap in the evaluation of drug-induced QT interval prolongation. *British Journal of Clinical Pharmacology* 76: 708-724.
- Charbit B, Alvarez JC, Dasque E, Abe E, Demolis JL, & Funck-Brentano C (2008). Droperidol and ondansetron-induced QT interval prolongation: a clinical drug interaction study. *Anesthesiology* 109: 206-212.
- Corey A, Agnew J, Brum J, Parekh N, Valentine S, & Williams M (1999). Pharmacokinetics and pharmacodynamics following intravenous doses of azimilide dihydrochloride. *J Clin Pharmacol* 39: 1263-1271.
- Dapo B, Benson C, Dota C, Ferber G, Gamett C, Green CL, *et al.* (2015). Results from the IQ-CSRC prospective study support replacement of the thorough QT study by QT assessment in the early clinical phase. *Clin Pharmacol Ther* 97: 326-335.
- Dixon R, Job S, Oliver R, Tompson D, Wright JG, Maltby K, *et al.* (2008). Lamotrigine does not prolong QTc in a thorough QT/QTc study in healthy subjects. *Br J Clin Pharmacol* 66: 396-404.
- Duchene-Marullaz P, Kantelip JP, & Trolese JF (1983). Effects of bepridil, a new antianginal agent, on ambulatory electrocardiography in human volunteers. *J Cardiovasc Pharmacol* 5: 506-510.
- Frnberg LE, Isbister GK, & Duffill SB (2006). Pharmacokinetic-pharmacodynamic modelling of QT interval prolongation following citalopram overdoses. *Br J Clin Pharmacol* 61: 177-190.
- Funck-Brentano C (1993). Pharmacokinetic and pharmacodynamic profiles of d-sotalol and d,l-sotalol. *Eur Heart J* 14 Suppl H: 30-35.
- Harrigan EP, Miceli JJ, Anziano R, Watsky E, Reeves KR, Cutler NR, *et al.* (2004). A randomized evaluation of the effects of six antipsychotic agents on QTc, in the absence and presence of metabolic inhibition. *J Clin Psychopharmacol* 24: 62-69.
- Honig PK, Wortham DC, Zamani K, Dp C, Mullin JC, & Cantilena LR (1993). Terfenadine-Ketoconazole Interaction - Pharmacokinetic and electrocardiographic consequences. *JAMA* 269: 1513-1518.
- Hough DW, Natarajan J, Vandebosch A, Rossem S, Kramer M, & Eerdeken M (2011). Evaluation of the effect of paliperidone extended release and quetiapine on corrected QT intervals: a randomized, double-blind, placebo-controlled study. *Int Clin Psychopharmacol* 26: 25-34.
- Hulhoven R, Rosillon D, Letiexhe M, Meeus MA, Daoust A, & Stockis A (2007). Levocetirizine does not prolong the QT/QTc interval in healthy subjects: results from a thorough QT study. *Eur J Clin Pharmacol* 63: 1011-1017.
- Johannesen L, Vicente J, Mason JW, Sanabria C, Waite-Labott K, Hong M, *et al.* (2014). Differentiating drug-induced multichannel block on the electrocardiogram: randomized study of dofetilide, quinidine, ranolazine, and verapamil. *Clin Pharmacol Ther* 96: 549-558.
- Jonker DM, Kenna LA, Leishman D, Wallis R, Milligan PA, & Jonsson EN (2005). A pharmacokinetic-pharmacodynamic model for the quantitative prediction of dofetilide clinical QT prolongation from human ether-a-go-go-related gene current inhibition data. *Clin Pharmacol Ther* 77: 572-582.

Katritsis D, Morgan J, Brachmann J, Bygrave A, O'Farrell D, Rowland E, *et al.* (1997). Electrophysiological effects of E 4031, a drug with selective class III properties, in man. *Pacing Clin Electrophysiol* 20: 930-937.

Noel G (2003). Effects of three fluoroquinolones on QT interval in healthy adults after single doses. *Clinical Pharmacology & Therapeutics* 73: 292-303.

Phillips L (2001). A population pharmacokinetic-pharmacodynamic analysis and model validation of azimilide. *Clinical Pharmacology & Therapeutics* 70: 370-383.

Platia EV, Weisfeldt ML, & Franz MR (1988). Immediate quantitation of antiarrhythmic drug effect by monophasic action potential recording in coronary artery disease. *Am J Cardiol* 61: 1284-1287.

Reiter MJ, Higgins SL, Payne AG, & Mann DE (1986). Effects of quinidine versus procainamide on the QT interval. *Am J Cardiol* 58: 512-516.

Salih IS, Thanacoody RH, McKay GA, & Thomas SH (2007). Comparison of the effects of thionidazine and mesonidazine on the QT interval in healthy adults after single oral doses. *Clin Pharmacol Ther* 82: 548-554.

Sedgwick M, Rasmussen HS, Walker D, & Cobbe SM (1991). Pharmacokinetic and pharmacodynamic effects of UK-68,798, a new potential class III antiarrhythmic drug. *Br J Clin Pharmacol* 31: 515-519.

Sweeney KR, Gastonguay MR, Benincosa L, Cronenberg CL, Glue P, & Malhotra BK (2010). Exposure-response modeling and clinical trial simulation of the effect of tolterodine on QT intervals in healthy volunteers. *Drug Discov Ther* 4: 44-53.

Thomas SH, Higham PD, Hartigan-Go K, Kamali F, Wood P, Campbell RW, *et al.* (1995). Concentration dependent cardiotoxicity of terodiline in patients treated for urinary incontinence. *Br Heart J* 74: 53-56.

Tisdale JE, Overholser BR, Wroblewski HA, Sowinski KM, Amankwa K, Borzak S, *et al.* (2012). Enhanced sensitivity to drug-induced QT interval lengthening in patients with heart failure due to left ventricular systolic dysfunction. *J Clin Pharmacol* 52: 1296-1305.

Uematsu T, Kanamaru M, & Nakashima M (1994). Comparative pharmacokinetic and pharmacodynamic properties of oral and intravenous (+)-sotalol in healthy volunteers. *J Pharm Pharmacol* 46: 600-605.

¹https://www.accessdata.fda.gov/drugsatfda_docs/nda/99/21-085_Avelox_medr_P8.pdf

²https://www.accessdata.fda.gov/drugsatfda_docs/nda/2017/209092Orig1s000MultidisciplineR.pdf

³https://www.accessdata.fda.gov/drugsatfda_docs/nda/2011/022405Orig1s000ClinPhamR.pdf

Table S3. References used in calculating effective free therapeutic plasma concentrations (EFTPC)

Compound	EFTPC (nM)	References		
		EFTPC	Total Plasma Exposure	Plasma Protein Binding
Alfuzosin	21		(Schulz, Iwersen-Bergmann, Andresen & Schmoldt, 2012)	www.drugbank.ca
Amitriptyline	41	(Redfem et al., 2003)		
Amlodipine	2	(Redfem et al., 2003)		
Astemizole	3.6		(Schulz, Iwersen-Bergmann, Andresen & Schmoldt, 2012)	www.drugbank.ca
Azimilide	70	(Redfem et al., 2003)		
Bepridil	33	(Redfem et al., 2003)		
Bupivacaine	260		(Schulz, Iwersen-Bergmann, Andresen & Schmoldt, 2012)	www.drugbank.ca
Carbamazepine	9481		(Schulz, Iwersen-Bergmann, Andresen & Schmoldt, 2012)	www.drugbank.ca
Chlorpromazine	38	(Redfem et al., 2003)		
Cisapride	3	(Redfem et al., 2003)		
Citalopram	68		(Schulz, Iwersen-Bergmann, Andresen & Schmoldt, 2012)	www.drugbank.ca
Clarithromycin	1206	(Redfem et al., 2003)		
Clomipramine	20		(Schulz, Iwersen-Bergmann, Andresen & Schmoldt, 2012)	www.drugbank.ca
Clozapine	71	(Kramer et al., 2013)		
Desipramine	108	(Redfem et al., 2003)		
Diltiazem	122	(Redfem et al., 2003)		
Disopyramide	742	(Redfem et al., 2003)		
Dofetilide	2	(Redfem et al., 2003)		
Domperidone	19	(Redfem et al., 2003)		
Droperidol	13		(Schulz, Iwersen-Bergmann, Andresen & Schmoldt, 2012)	www.drugbank.ca
E-4031	6	(Okada et al., 2015)		
Felodipine	0.3		(Schulz, Iwersen-Bergmann, Andresen & Schmoldt, 2012)	www.drugbank.ca
Flecainide	753	(Redfem et al., 2003)		
Halofantrine	172	(Kramer et al., 2013)		
Ibutilide	140	(Redfem et al., 2003)		
Imipramine	106	(Redfem et al., 2003)		
Isradipine	0.3		(Schulz, Iwersen-Bergmann, Andresen & Schmoldt, 2012)	www.drugbank.ca
Lamotrigine	24601		(Schulz, Iwersen-Bergmann, Andresen & Schmoldt, 2012)	www.drugbank.ca
Levocetirizine	104		(Schulz, Iwersen-Bergmann, Andresen & Schmoldt, 2012)	www.drugbank.ca
Levofloxacin	23104		[†] FDA Documentation	www.drugbank.ca
Loratadine	0.5	(Redfem et al., 2003)		
Manidipine	0.1	(Stockis et al., 2003)		
Maprotiline	130	(Redfem et al., 2003)		
Mesoridazine	2483		(Schulz, Iwersen-Bergmann, Andresen & Schmoldt, 2012)	www.drugbank.ca
Metoprolol	1664		(Schulz, Iwersen-Bergmann, Andresen & Schmoldt, 2012)	www.drugbank.ca
Mexiletine	4129	(Redfem et al., 2003)		
Moxifloxacin	10960	(Kramer et al., 2013)		
Nicardipine	10		(Schulz, Iwersen-Bergmann, Andresen & Schmoldt, 2012)	www.drugbank.ca
Nifedipine	8	(Redfem et al., 2003)		
Nilvadipine	0.5		(Schulz, Iwersen-Bergmann, Andresen & Schmoldt, 2012)	(Niwa, Tokuma & Noguchi, 1987)
Nimodipine	6		(Schulz, Iwersen-Bergmann, Andresen & Schmoldt, 2012)	www.drugbank.ca
Nitrendipine	3	(Redfem et al., 2003)		
Nortriptyline	53		(Schulz, Iwersen-Bergmann, Andresen & Schmoldt, 2012)	www.drugbank.ca
Ondansetron	156	[†] FDA Documentation		
Paliperidone	69	(Kramer et al., 2013)		
Pentamidine	455		(Schulz, Iwersen-Bergmann, Andresen & Schmoldt, 2012)	www.drugbank.ca
Pimozide	1.0	(Redfem et al., 2003)		
Procainamide	54180	(Redfem et al., 2003)		
Procaine	9945		(Schulz, Iwersen-Bergmann, Andresen & Schmoldt, 2012)	(Covino, 1986)
Propafenone	241	(Redfem et al., 2003)		
Quinidine	3237	(Redfem et al., 2003)		
Quinine	6473		(Schulz, Iwersen-Bergmann, Andresen & Schmoldt, 2012)	www.drugbank.ca
Ranolazine	1948	(Crumb, Vicente, Johannesen & Strauss, 2016)		
Ribociclib	547		(Samant et al., 2018)	[†] FDA Documentation
Risperidone	2	(Redfem et al., 2003)		
Ropivacaine	612	[†] FDA Documentation		
Sertindole	2	(Redfem et al., 2003)		
Sotalol	14690	(Redfem et al., 2003)		
Tamoxifen	21	(Redfem et al., 2003)		
Terfenadine	9	(Redfem et al., 2003)		
Terodiline	266	(Langtry & McTavish, 1990)		
Thioridazine	270		(Schulz, Iwersen-Bergmann, Andresen & Schmoldt, 2012)	www.drugbank.ca
Tolterodine	2.2		[†] FDA Documentation	www.drugbank.ca
Vandetanib	255	[†] FDA Documentation		
Venlafaxine	1009		(Schulz, Iwersen-Bergmann, Andresen & Schmoldt, 2012)	www.drugbank.ca
Verapamil	81	(Redfem et al., 2003)		

References

- Covino BG (1986). Pharmacology of local anaesthetic agents. *Br J Anaesth* 58: 701-716.
- Crumb WJ, Jr., Vicente J, Johannesen L, & Strauss DG (2016). An evaluation of 30 clinical drugs against the comprehensive in vitro proarrhythmia assay (CiPA) proposed ion channel panel. *J Pharmacol Toxicol Methods* 81: 251-262.
- Kramer J, Obejero-Paz CA, Myatt G, Kuryshev YA, Bruening-Wright A, Verducci JS, *et al.* (2013). MICE models: superior to the HERG model in predicting Torsade de Pointes. *Sci Rep* 3: 2100.
- Langtry HD, & McTavish D (1990). Terodiline. A review of its pharmacological properties, and therapeutic use in the treatment of urinary incontinence. *Drugs* 40: 748-761.
- Niwa T, Tokuma Y, & Noguchi H (1987). Plasma protein binding of nilvadipine, a new dihydropyridine calcium antagonist, in man and dog. *Res Commun Chem Pathol Pharmacol* 55: 75-88.
- Okada J, Yoshinaga T, Kurokawa J, Washio T, Furukawa T, Sawada K, *et al.* (2015). Screening system for drug-induced arrhythmogenic risk combining a patch clamp and heart simulator. *Sci Adv* 1: e1400142.
- Redfern WS, Carlsson L, Davis AS, Lynch WG, MacKenzie I, Palethorpe S, *et al.* (2003). Relationships between preclinical cardiac electrophysiology, clinical QT interval prolongation and torsade de pointes for a broad range of drugs: evidence for a provisional safety margin in drug development. *Cardiovasc Res* 58: 32-45.
- Samant TS, Dhuria S, Lu Y, Laisney M, Yang S, Grandeur A, *et al.* (2018). Ribociclib Bioavailability Is Not Affected by Gastric pH Changes or Food Intake: In Silico and Clinical Evaluations. *Clin Pharmacol Ther* 104: 374-383.
- Schulz M, Iwersen-Bergmann S, Andresen H, & Schmoldt A (2012). Therapeutic and toxic blood concentrations of nearly 1,000 drugs and other xenobiotics. *Crit Care* 16: R136.
- Stockis A, De Bruyn S, Gengler C, Goethals F, Lens S, Poli G, *et al.* (2003). Pharmacokinetics and tolerability of a new manidipine and delapril fixed oral combination in young and elderly subjects. *Arzneimittelforschung* 53: 554-561.
- ¹FDA Documentation: www.accessdata.fda.gov/drugsatfda_docs/label/2010/020007s040,020403s0181bl.pdf
- ²FDA Documentation: www.accessdata.fda.gov/drugsatfda_docs/label/2018/020533s0351bl.pdf
- ³FDA Documentation: www.accessdata.fda.gov/drugsatfda_docs/nda/2011/022405Orig1s000ClinPhamR.pdf
- ⁴FDA Documentation: www.accessdata.fda.gov/drugsatfda_docs/label/2008/021721s020_020635s57_020634s52_1bl.pdf
- ⁵FDA Documentation: https://www.accessdata.fda.gov/drugsatfda_docs/label/2009/020771s0221bl.pdf
- ⁶FDA Documentation: www.accessdata.fda.gov/drugsatfda_docs/label/2019/209092s0041bl.pdf

Table S4. References defining Torsades de Pointes (TdP) risk categories

Compound	TdP Risk Category	Reference
Alfuzosin	3	Woosley et al.
Amitriptyline	2	Woosley et al.
Amlodipine	4	No literature evidence of TdP
Astemizole	1	Woosley et al.
Azimilide	1	Colatsky et al.
Bepriidil	1	Woosley et al.
Bupivacaine	4	No literature evidence of TdP
Carbamazepine	4	No literature evidence of TdP
Chlorpromazine	1	Woosley et al.
Cisapride	1	Woosley et al.
Citalopram	1	Woosley et al.
Clarithromycin	1	Woosley et al.
Clomipramine	2	Woosley et al.
Clozapine	3	Woosley et al.
Desipramine	3	Woosley et al.
Diltiazem	4	Colatsky et al.
Disopyramide	1	Woosley et al.
Dofetilide	1	Woosley et al.
Domperidone	1	Woosley et al.
Droperidol	1	Woosley et al.
E-4031	1	Goto et al.
Felodipine	4	No literature evidence of TdP
Flecainide	1	Woosley et al.
Halofantrine	1	Woosley et al.
Ibutilide	1	Woosley et al.
Imipramine	3	Woosley et al.
Isradipine	3	Woosley et al.
Lamotrigine	4	No literature evidence of TdP
Levocetirizine	4	No literature evidence of TdP
Levofloxacin	1	Woosley et al.
Loratadine	4	Colatsky et al.
Manidipine	4	No literature evidence of TdP
Maprotiline	3	Woosley et al.
Mesoridazine	1	Woosley et al.
Metoprolol	4	Colatsky et al.
Mexiletine	4	Colatsky et al.
Moxifloxacin	1	Woosley et al.
Nicardipine	3	Woosley et al.
Nifedipine	4	Colatsky et al.
Nilvadipine	4	No literature evidence of TdP
Nimodipine	4	No literature evidence of TdP
Nitrendipine	4	Colatsky et al.
Nortriptyline	3	Woosley et al.
Ondansetron	1	Woosley et al.
Paliperidone	3	Woosley et al.
Pentamidine	1	Woosley et al.
Pimozide	1	Woosley et al.
Procainamide	1	Woosley et al.
Procaine	4	No literature evidence of TdP
Propafenone	2	Woosley et al.
Quinidine	1	Woosley et al.
Quinine	2	Woosley et al.
Ranolazine	2	Woosley et al.
Ribociclib	3	Woosley et al.
Risperidone	2	Woosley et al.
Ropivacaine	4	No literature evidence of TdP
Sertindole	1	Woosley et al.
Sotalol	1	Woosley et al.
Tamoxifen	3	Woosley et al.
Terfenadine	1	Woosley et al.
Terodiline	1	Woosley et al.
Thioridazine	1	Woosley et al.
Tolterodine	3	Woosley et al.
Vandetanib	1	Woosley et al.
Venlafaxine	3	Woosley et al.
Verapamil	4	Colatsky et al.

Risk Definitions

Drugs were categorized into one of 4 risk categories as defined below. Categories 1- 3 utilized the risk definitions defined by crediblemeds.org (Woosley et al.). An additional risk category (category 4) was used to define risk for drugs not categorized by crediblemeds.org that were either defined as low risk by cipaproject.org (Colatsky et al., 2016) or that have no clear literature evidence of associated TdP risk.

1. Drugs that prolong the QT interval AND are clearly associated with a known risk of TdP, even when taken as recommended (including azimilide (Colatsky et al., 2016) and E-4031 (Goto et al., 2018) that are not described in crediblemeds.org).
2. Drugs that are associated with TdP BUT only under certain conditions of their use (e.g. excessive dose, in patients with conditions such as hypokalemia, or when taken with interacting drugs) OR by creating conditions that facilitate or induce TdP (e.g. by inhibiting metabolism of a QT-prolonging drug or by causing an electrolyte disturbance that induces TdP.)
3. Drugs that can cause QT prolongation BUT currently lack evidence for a risk of TdP when taken as recommended
4. Drugs not categorized by crediblemeds.org that were either defined as low risk by cipaproject.org or that have no clear literature evidence of associated TdP risk.

References

- Colatsky T, Femini B, Gintant G, Pierson JB, Sager P, Sekino Y, et al. (2016). The Comprehensive in Vitro Proarrhythmia Assay (CiPA) initiative - Update on progress. *J Pharmacol Toxicol Methods* 81: 15-20.
- Goto A, Izumi-Nakaseko H, Hagiwara-Nagasawa M, Chiba K, Ando K, Naito AT, et al. (2018). Analysis of torsadogenic and pharmacokinetic profile of E-4031 in dogs bridging the gap of information between in vitro proarrhythmia assay and clinical observation in human subjects. *J Pharmacol Sci* 137: 237-240.
- Woosley RL, Heise CW, Gallo T, Tate J, Woosley D and Romero KA. www.CredibleMeds.org. QTdrugs List, [Accession Date: 8th February 2021], AZCERT, Inc. 1822 Innovation Park Dr., Oro Valley, AZ 85755.